JOURNAL OF GEOPHYSICAL RESEARCH, VOL. 104, NO. C9, PAGES 21,171–21,194, SEPTEMBER 15, 1999

Intercomparison of the upper layer circulation of the western equatorial Atlantic Ocean: In situ and satellite data

S. Arnault

Laboratoire d'Océanographie Dynamique et de Climatologie, Unité Mixte de Recherche 7617 Centre National de Recherche Scientifique/Institut de Recherche pour le Développement/Université Pierre et Marie Curie, Paris, France

B. Bourlès, Y. Gouriou, and R. Chuchla

Centre Institut de Recherche pour le Développement de Brest, Plouzané, France

Abstract. Thanks to the agreement found between in situ measurements and TOPEX/POSEIDON data in the western tropical Atlantic Ocean, a realistic picture of the spatial and temporal variability over the 1992-1997 period is obtained. The sea level variability clearly emphasizes three ranges of variability. The intraseasonal variability is associated with propagating features north of the equator, consistent with a first baroclinic Rossby wave characteristic. The annual variability, which represents the largest part of the variability, describes the seasonal cycle of the North Equatorial Countercurrent; but, more interesting, is a clear year-to-year variability in the northernmost part of the area. The surface currents also reveal an intraseasonal tendency with a peak of energy at 62 days at 5°N. Upper layer volume transport across 38°W and between 3°N and 9°N shows a regular seasonal contrast mostly due to the 3°N-6°N region. Year-to-year variations are also clearly evidenced. The eastward transport loses about 35% of its strength in the second half of 1995 compared with 1994. This event is followed by a stronger than usual westward transport in early 1996, and in early 1997, the transport seems abnormally eastward. However, contrary to the seasonal cycle, this interannual variability occurs mainly in the 6°N-9°N band. Interhemispheric transport computed across 7°30'N, between 50°W and 35°W, is northward during the whole period 1992-1995. A seasonal cycle can be detected with maximum transport during boreal winter and minimum in spring. An interesting result is the increasing tendency of the northward transport from April 1993 until boreal fall 1995, when the maximum value for the period is reached.

1. Introduction

During the last 10-15 years, thanks to different oceanographic programs such as the Français Océan Climat en Atlantique Équatorial/Seasonal EquatoriaL Atlantic (FOCAL/SEQUAL), Tropical Ocean Global Atmosphere (TOGA), and World Ocean Circulation Experiment (WOCE) programs, data analysis as well as numerical modeling studies have evidenced the complexity of the tropical Atlantic Ocean variability. In contrast to the Pacific, where ocean fluctuations are predominantly on seasonal to interannual timescales, the variability of the Atlantic appears on intraseasonal, seasonal, and interannual scales and also on a characteristic decadal (and even longer) time period usually associated with the "conveyor belt" [*Gordon*, 1986]. The northernmost Atlantic extent favors surface waters to become increasingly salty and to sink as they flow in from the Southern Ocean, and the incoming waters are compensated by the outflow of deep water. Cross-equatorial heat and salt fluxes are required to realize this climatic Atlantic signal. Although schematic diagrams of average currents in the tropical Atlantic have been constructed in previous studies [*Richardson et al.*, 1994], questions about that circulation are still pending, such as, for example, the different pathways of cross-equatorial transports.

Numerical studies of the tropical Atlantic Ocean have revealed that most of the northward flux of heat and mass should be concentrated on the western boundary. Western boundary currents are the most powerful currents in the oceans. No wind-driven ocean circulation theory is complete without the closure of the western boundary; but the complexity stems from the huge spatial extent of those currents and from their tremendous spatial and temporal variability. Early modeling studies indicated that the advection of South Atlantic waters into the subtropical gyre of the North Atlantic was the result of a continuous western boundary transport [*Philander and Pacanowski*, 1986]. However, results from the WOCE community modeling effort do not present such an important direct transport along this route [*Schott and Boning*, 1991]. Furthermore, recent observations indicate that some transport occurs along the western boundary via intermittent shallow boundary currents and eddies that pinch off from the North Brazil Current (NBC) Retroflection [*Richardson et al.*, 1994; *Bourlès et al.*, 1999; *Johns et al.*, 1998]. Indeed, the difficulties are compounded by the fact that these regions are the spawning areas for mesoscale eddy activities. As stated by *Johns et al.* [1998], possible pathways for the northward flow at the western boundary surface should include a coastal

Paper number 1999JC900124.
0148-0227/99/1999JC900124$09.00

boundary current [*Csanady,* 1985; *Candela et al.,* 1992; *Friedrich and Hall,* 1993; B. Bourlès et al., manuscript in preparation, 1999], rings shed from the NBC Retroflection, and offshore NBC Retroflection into the North Equatorial Countercurrent (NECC) followed by northward Ekman transport [*Mayer and Weisberg,* 1993].

Thus the mechanisms that carry the western boundary throughflow have yet to be fully documented. As numerical models, in general, in particular in the tropics, are very sensitive to inaccuracies in surface forcings and parameterized model physics [*Blanke and Delecluse,* 1993; *Bryan et al.,* 1995], high-quality climate data sets are still needed. Another interesting aspect is the combined use of satellite observations with in situ data.

As part of the WOCE program, two oceanographic cruises were carried out in the western tropical Atlantic Ocean: ETAMBOT 1 in September-October 1995 and ETAMBOT 2 in April-May 1996. High-quality in situ measurements were gathered west of 35°W, between 5°S and 10°N, along three sections at 7°30'N, 35°W and a slanted section (hereinafter referred to as the Ceara transect) from the Amazon mouth (0°N,45°W) to 8°N,41°W, crossing the Ceara Rise. Different parameters sampled during the cruises are described by the following: *Andrié et al.* [this issue] analyze the deep flows from CFCs and tracer data, *Oudot et al.* [this issue] describe the Antarctic Intermediate Water (AAIW) through nutrients, *Bourlès et al.* [this issue] present a description of the upper layer circulation and transports during the cruises from ship-mounted acoustic Doppler current profiler (SADCP) and hydrographic data, and *Gouriou et al.* [this issue] describe (from lowered ADCP, LADCP) the deep jets occurring along the equator.

In this study, we use the ETAMBOT data together with the TOPEX/POSEIDON altimetric measurements in order to obtain information about the variability of sea level, currents, and transports in that western boundary area. Previous encouraging altimetric studies have been carried out with the 17-day cycle and the 2-year duration of the Geosat altimeter mission on the seasonal cycle of the NECC and NBC [*Carton and Katz,* 1990; *Didden and Schott,* 1992, 1993]. Thanks to the longer TOPEX/POSEIDON time series and higher sea level accuracy and the concomitant ETAMBOT data sets, we pursue herein these preliminary efforts. We investigate larger temporal scale fluctuations of velocity and fluxes in order to place the cruise in a more general temporal and spatial context and to bring complementary information on the dynamics mentioned above.

After reviewing data processing for both in situ and satellite observations, the quality of the TOPEX/POSEIDON signal in that area is first investigated by comparison with in situ ETAMBOT measurements. Then, we analyze and discuss the sea level, current and transport variability obtained by TOPEX/POSEIDON over the 1992-1997 period, before offering conclusions.

2. Data Processing

2.1 Altimetric Data

Cycles 5 to 186, November 1992 to October 1997, of TOPEX/POSEIDON geophysical data records were processed over the tropical Atlantic Ocean from 80°W to 20°E and 45°N to 45°S in order to obtain sea level anomalies (SLAs) referenced to a mean profile. This reference to a mean profile, which is dominated by geoid undulations and stationary oceanic circulation, is necessary in order to eliminate unknown marine geoid information. Standard corrections for the troposphere, ionosphere, inverse barometer, and sea state bias were applied. We used the Texas University tide model (version CSR3) for tide corrections. Recently, *Arnault and LeProvost* [1997] demonstrated that using either the Texas University tide model or the Grenoble University tide model leads to the same residual tide error effect on the sea level variability in the western tropical Atlantic: a strong 2-month residual error with a 5- to 6-cm amplitude is located offshore from the Amazon river, and a weaker signal (3 cm) is concentrated on the continental shelf up to the Caribbean. Thus we will only refer to the altimetric data offshore of the 500-m isobath. Erroneous data with SLAs greater than 50 cm were also discarded from the analysis.

The original altimetric sampling of TOPEX/POSEIDON data is about 7 km along track over a 10-day repeat cycle. Along the equator, two adjacent tracks are spaced 350 km apart. Obviously, this is not enough for the description of mesoscale variability features. Thus an objective analysis [*Bretherton et al.,* 1976] has been performed on the data to interpolate them on a regular 0.5° x 0.5° x 5-day grid between 55°W,30°W and 10°N,10°S. This kind of approach has already been used successfully in altimetric studies [*De Mey and Robinson,* 1987; *Mallardé et al.,* 1987; *Arnault et al.,* 1990]. An isotropic correlation radius of 200 km was assumed together with a 15-day temporal correlation. Owing to the high precision of TOPEX/POSEIDON data, in particular of the TOPEX/POSEIDON orbit, the mean accuracy of SLA is about 2 cm. Geostrophic currents were then computed from SLA 1° off the equator using a finite difference scheme and the geostrophic balance:

$$U = -g/f\, \partial h/\partial y \qquad (1)$$

$$V = g/f\, \partial h/\partial x$$

where U, V are the zonal and meridional velocity components respectively; g is Earth's gravity; h is sea level; and f is the Coriolis parameter. From the 2-cm error assumed for the SLA, the errors in geostrophic velocity range from +/-30 cm s^{-1} near the equator to +/-5 cm s^{-1} around 7°30'N.

2.2 In Situ Measurements

More than 80 hydrographic casts were sampled during each of the September-October 1995 (ETAMBOT 1) and April-May 1996 (ETAMBOT 2) cruises (Figures 1a and 1b). Each station was about 55 km apart, except over the continental shelf and bathymetric rises, where the spacing was reduced. A complete description of the data processing and calibration is given by *Le Groupe ETAMBOT* [1997a, b]. We used the calibrated conductivity-temperature-depth (CTD) temperature and salinity profiles to calculate 0/500 dbar dynamic heights (DHs). In doing that, we assumed that the surface signature of motions below 500 dbar is weak or constant so that the 0/500 dbar DH could be efficiently compared with satellite altimetry. Several authors have demonstrated that the 0-500 dbar layer, which involves all the thermocline variability, clearly reflects most of the tropical Atlantic dynamics and that high-order baroclinic phenomena are generally of lesser importance [*Merle and Arnault,* 1985; *Carton and Katz,* 1990]. We investigated how

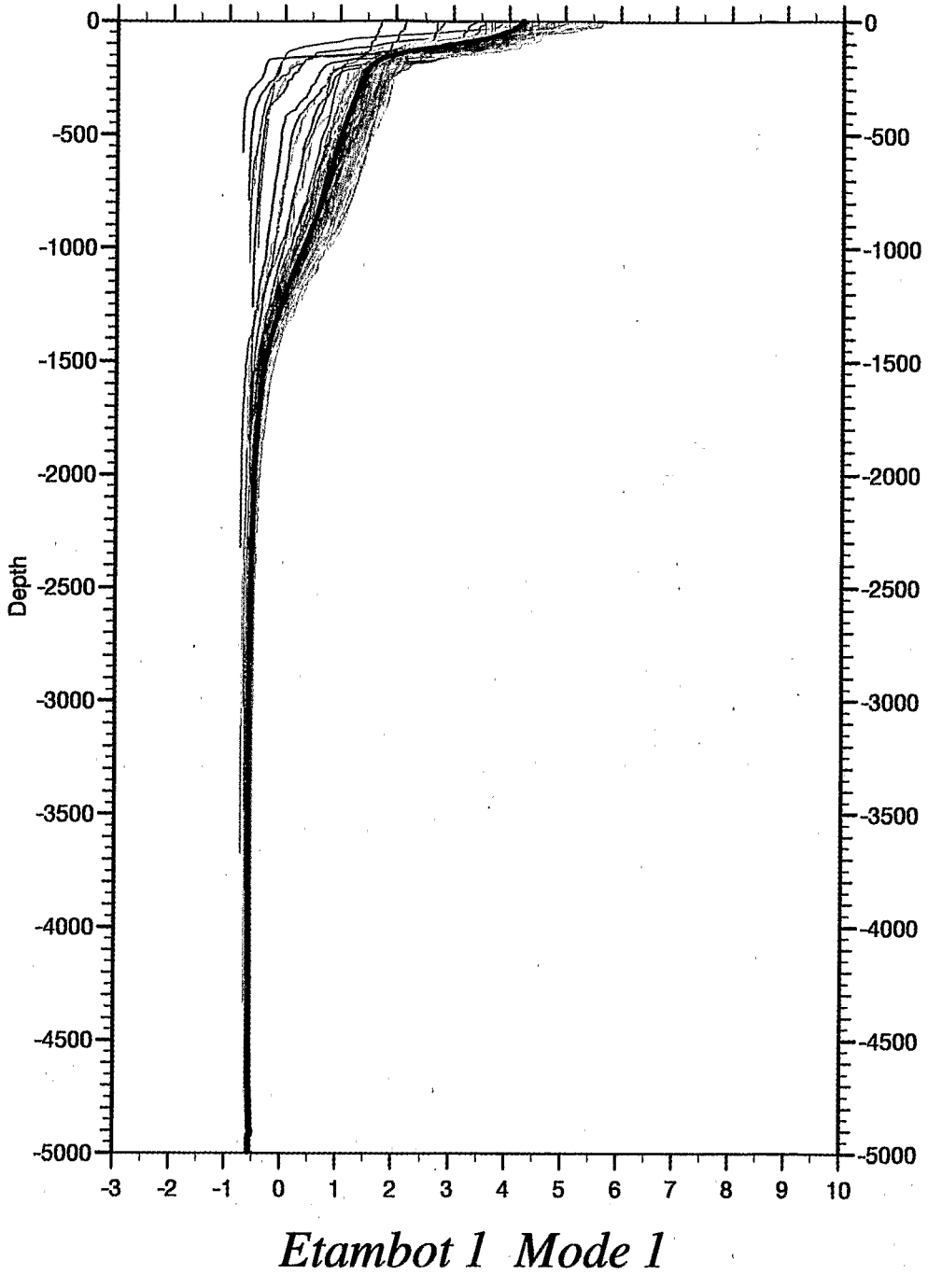

Plate 1. Mean vertical profiles obtained during (a) ETAMBOT 1 in September-October 1995 for the vertical mode 1 (M_1), (b) ETAMBOT 2 in April-May 1996 for M_1, (c) ETAMBOT 1 for vertical mode 2 (M_2), and (d) ETAMBOT 2 for M_2. The different colors are associated with the different transects of the cruises as follows: pink for 7°30'N, blue for 35°W, orange for Ceara, and purple for the stations offshore French Guiana. The bold profiles represent the mean vertical profile obtained for M_1 and M_2 from the whole data set.

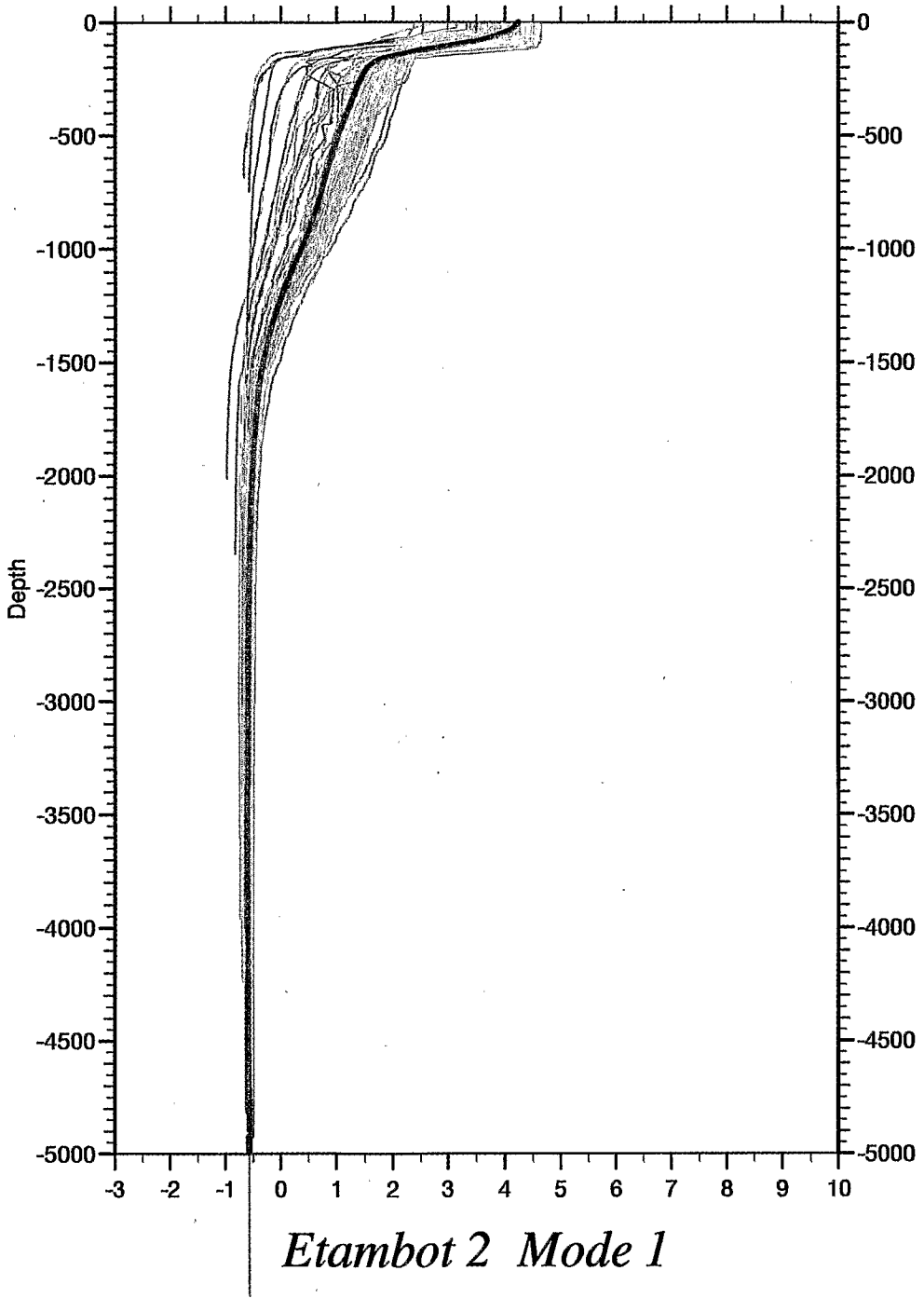

Plate 1. (continued)

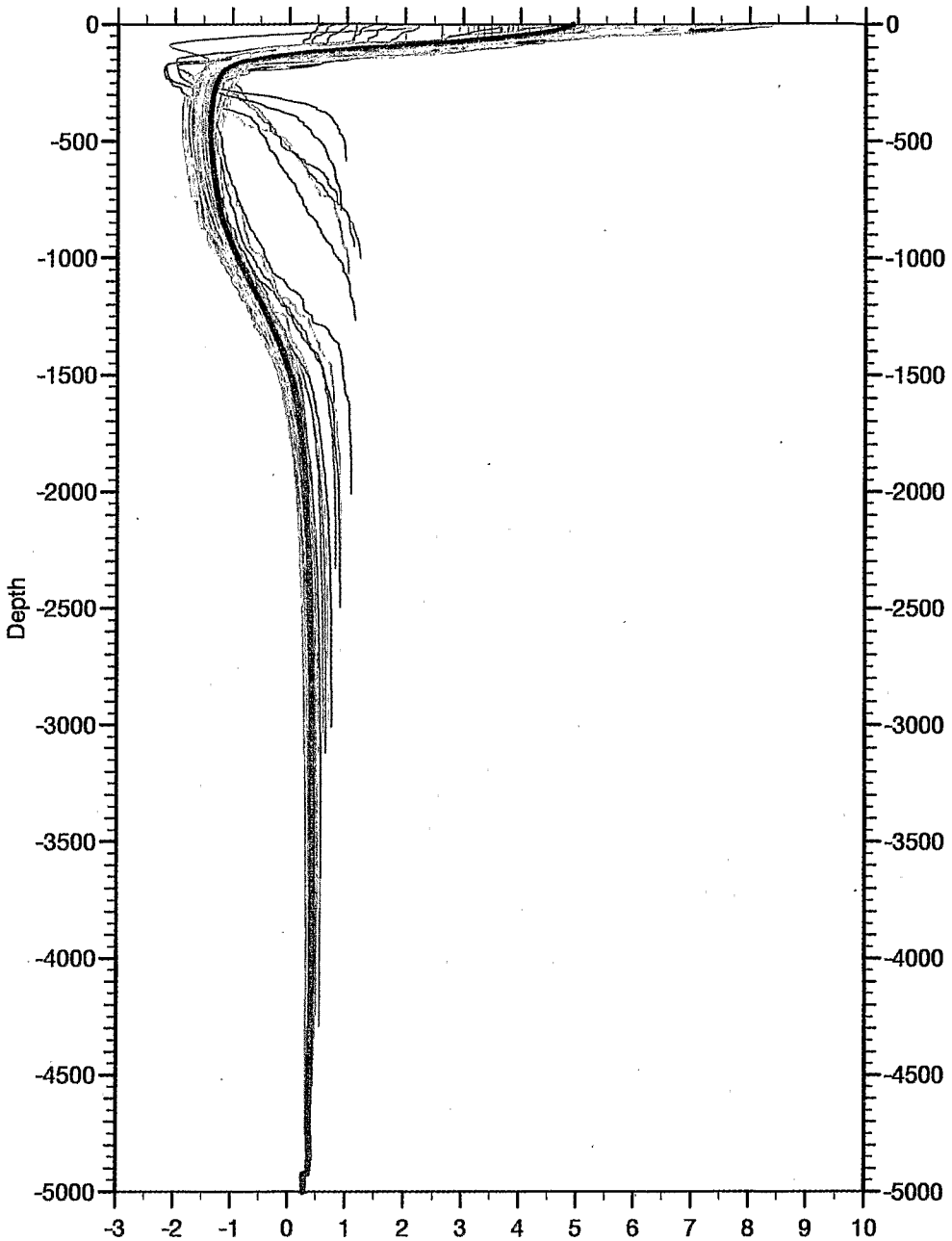

Plate 1. (continued)

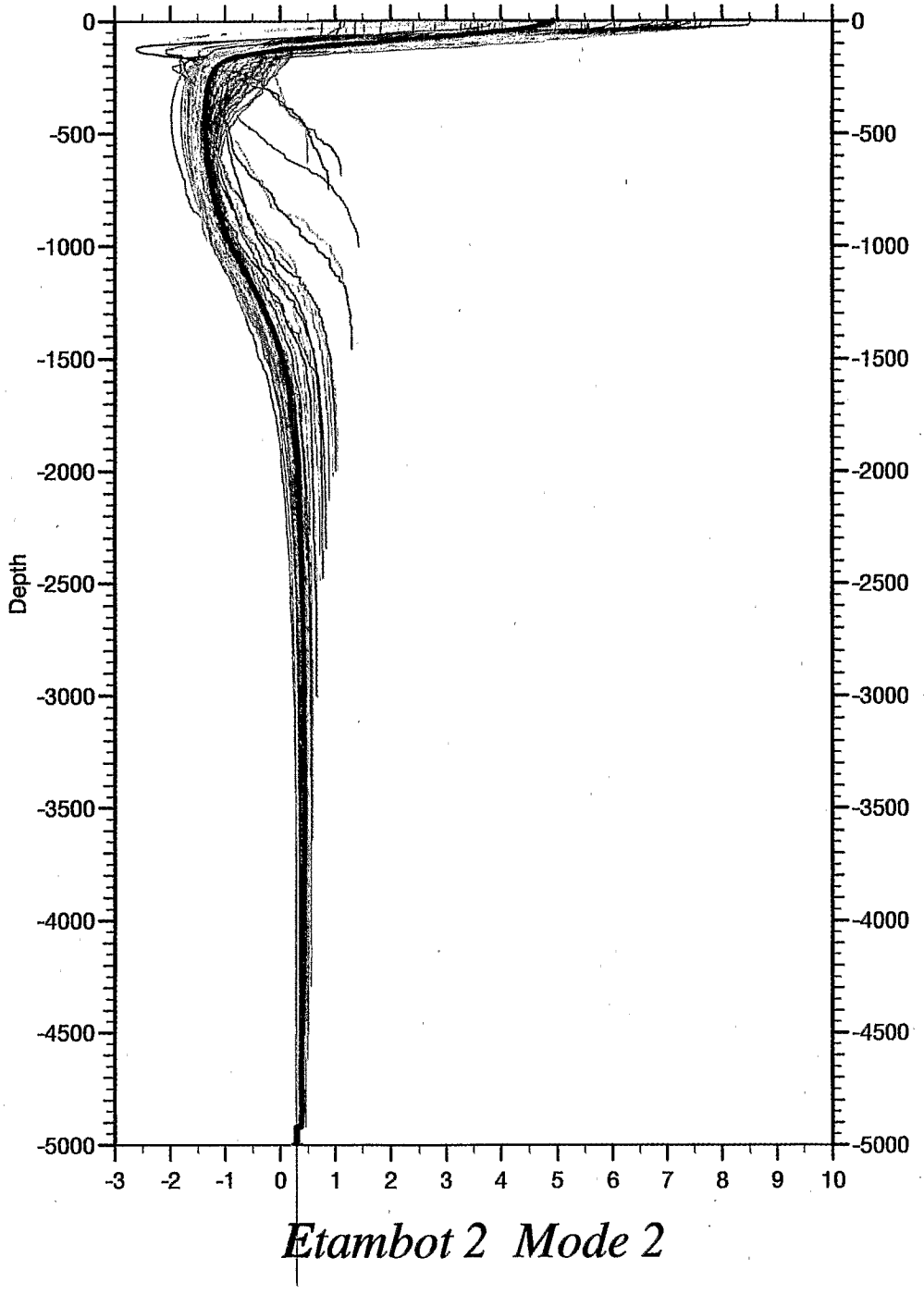

Plate 1. (continued)

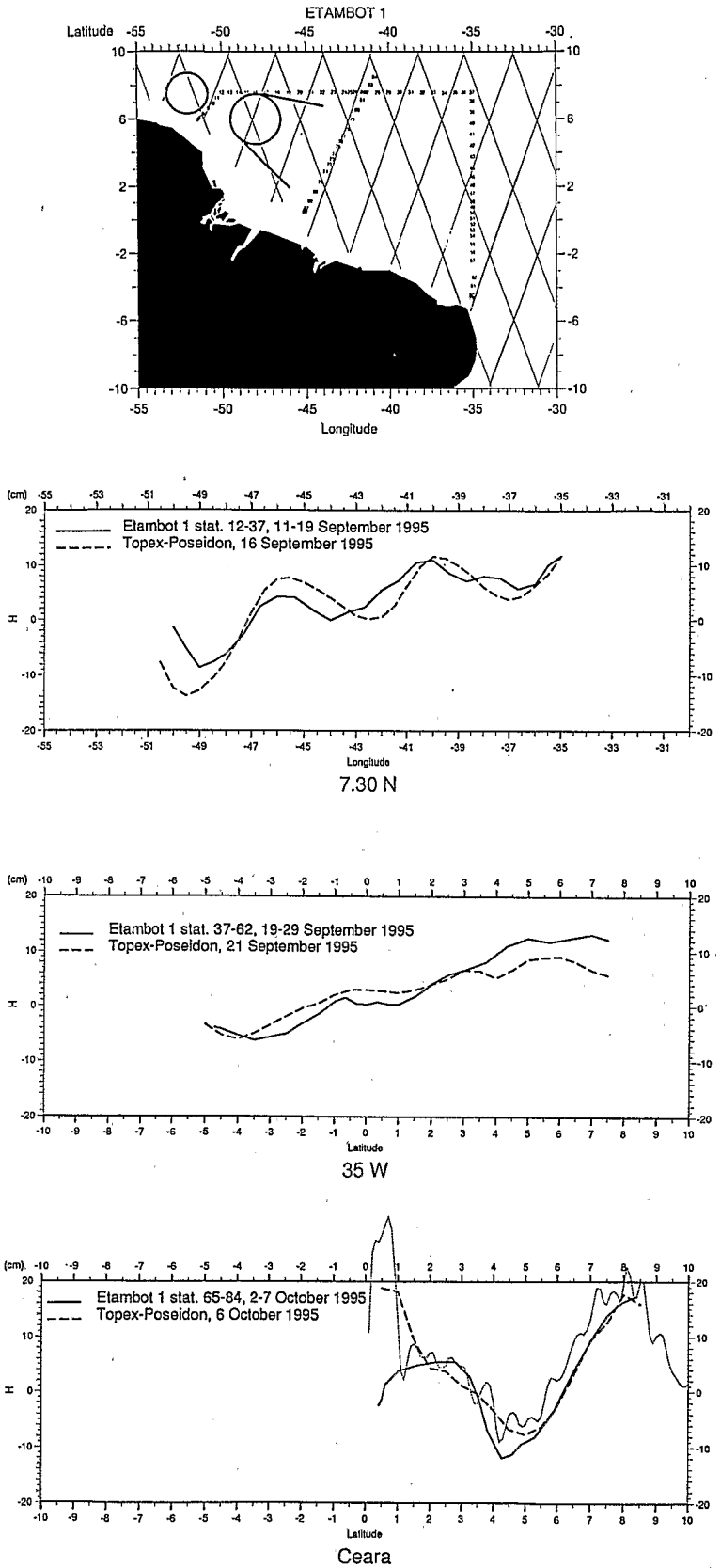

Figure 1a. (top) Ship route and hydrographic stations during ETAMBOT 1 in September-October 1995 together with altimetric ascending and descending tracks. A schematic North Equatorial Countercurrent/North Brazil Current retroflection and eddy structure have been mapped. Also shown are: sea level anomalies (SLAs) (in cm) and dynamic height anomalies (DHAs) (in dynamic cm (dyn. cm)) obtained from TOPEX/POSEIDON and the hydrographic data (referred to Levitus' climatology [*Levitus and Boyer*, 1994; *Levitus et al.*, 1994]) along the 7°30'N, 35°W and across the Ceara sections. The thin line for the Ceara diagram represents the raw along-track altimetric data (track 189, cycle 110). The mean rms difference is about 3 cm. The geographical locations discussed most often in text are the Amazon River, at the equator; the French Guiana, starting at 5°N; and the Ceara Rise, 40°W,3°N and 45°W,7°N

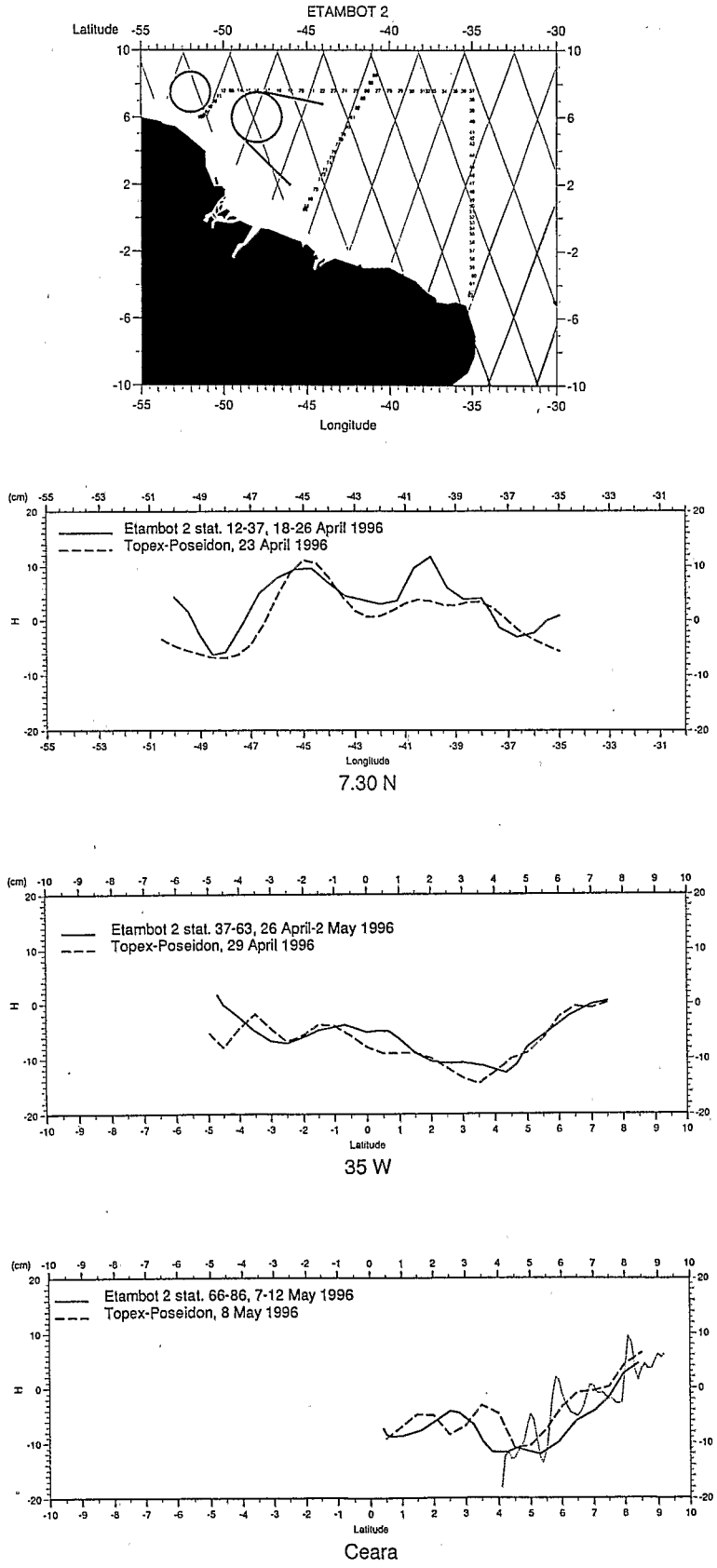

Figure 1b. Same as Figure 1a, except for ETAMBOT 2 cruise in April-May 1996 (cycle 132).

the surface DH patterns were sensitive to this choice by varying this reference level to deeper (up to 3000 dbar) levels. If any dynamics of importance for the purpose is missed by the 0/500 dbar DH and, on the contrary, is revealed by 0/3000 dbar DH, then the correlations between the different DHs will be low. In fact, the geographical correlations between the different surface DH signals are over 0.99. Thus the zonal and meridional gradients obtained using either 0/500 dbar DH or deeper referenced DH will not differ much. We kept this 500 dbar as the reference level, which constitutes a good compromise between the absolute "no-motion level" and the desire to keep the maximal number of CTD casts. Owing to the high accuracy of the CTD temperature and salinity measurements (+/- 0.005°C for temperature, +/-0.003 practical salinity unit (psu) for salinity), we assume the 0/500 dbar DH accuracy to be less than 1 dynamic centimeter (dyn. cm). We also need a climatology to reference the in situ measurements in the same way as the SLA is referenced to a mean altimetric profile. We use the Levitus data [*Levitus and Boyer,* 1994; *Levitus et al.,* 1994] to calculate climatological DHs, which, when subtracted from the ETAMBOT DHs, give the DH anomalies (DHAs).

The SADCP measurements provide another tool for altimetric comparison. Most of them have been collected continuously along the ship routes. The original 5-min velocity profiles have been averaged in "on-station" mean velocity profiles, and the accuracy of these data is below 5 cm s^{-1}. *Bourlès et al.* [this issue] assume a mean value of 3 cm s^{-1} for the surface layer accuracy. Similar to the comparison between SLA and DHA, a climatology based on ship drift data [*Richardson and McKee,* 1984] and Levitus geostrophic currents is used to calculate "absolute" currents.

3. ETAMBOT Cruise Comparisons

3.1. Sea Level Variability

The comparison of the TOPEX/POSEIDON SLA with the ETAMBOT DHA along the main ship lines is given in Figures 1a and 1b, together with the ship route and altimetric tracks. The agreement is visually good, especially along the longest sections at 7°30'N and 35°W. In September-October 1995 (Figure 1a), SLA and DHA exhibit at 7°30'N a zonal slope with minimal values around 49°W (-10 cm) and maximal values at 35°W (+10 cm). Superimposed on the west-east slope, both data sets evidence a succession of highs and lows with a correlation of 0.88 (0.79-0.94) and a wavelength of about 600 km. Mean zonal wavelengths observed in the past for such phenomena range between 390 and 740 km [*McClean and Klinck,* 1995]. The amplitude of this signal grows westward to reach more than 20 cm (peak to peak) at the westernmost stations. The root-mean-square (rms) difference between SLA and DHA is 3.4 cm, but a large part is due to the 10-cm misfit occurring between DHA and SLA at 50°W, near the coast. If we omit only this geographical point from the series, then the rms difference decreases to 2.5 cm, nearly equal to the TOPEX/POSEIDON accuracy. Along 35°W, DHA and SLA show a meridional slope starting from -6 cm at 3-4°S up to 10 cm at 7°N. However, this slope is steeper for the in situ data than for the altimetric measurements, resulting in a 3-cm rms difference. Along the Ceara transect, a V-shaped structure (and thus an inversion of the geostrophic cross-track velocity anomaly at about 5°N) appears with minimum values at 4°N (-10 cm) and maximum values at 2°30'N (about 5 cm) and 8°N (about 15 cm). The agreement is excellent (2.4 cm for the rms difference), except for the southernmost part of the section. Indeed, at 0.5°N, DHA opposes the increasing trend shown by SLA. As mentioned in section 2 and can be seen from the raw along-track data superimposed on the Ceara transect (thin line in Figure 1a, bottom), this is clearly the signature of local influence of tide corrections in the altimetric signal.

In April-May 1996 (Figure 1b) the zonal slope observed along 7°30'N during the preceding boreal fall cruise has disappeared or even slightly reversed between 45°W (+10 cm) and 35°W (-5 cm), but the undulations still persist. However, one of the DHA highs at 40°W has been missed by altimetry, so that the rms difference is about 4 cm. Along 35°W, both DHA and SLA present a decreasing trend from 5°S to 3°N, then a reversal and steep slope up to 7°N. The rms difference is below 2 cm, i.e., below the TOPEX/POSEIDON accuracy. Along the Ceara transect, DHA and SLA present the same large-scale tendency, but the small-scale structures along the southern part of the transect are clearly opposite. However, the TOPEX/POSEIDON values along that southern part of the track must be viewed with caution owing to isolated ionospheric correction problems for this particular period and geographical area. Then, from 5°N to 8°30'N, the agreement between DHA and SLA is attained again with the same increasing slope from -10 to 6 cm.

Thus this first comparison of SLA/DHA brings encouraging results. Thanks to the high quality of the TOPEX/POSEIDON altimetric measurements, mesoscale information as well as large-scale variability can be extracted from the satellite data through the means of an objective analysis and compares favorably with the ETAMBOT measurements. We now investigate in the next subsection if the agreement is still good in terms of current variability.

3.2. Surface Current Variability

Figures 2a and 2b present the comparison of the SADCP current measurements obtained at 16 m (SADCP first depth measurements) during the cruises with the surface velocities computed from altimetry. As anticipated from the previous comparison, the general agreement is rather good, especially along the meandering NECC at 7°30'N. During both cruises the undulations of SLA and DHA along 7°30'N result in alternating behavior of the currents. These features seem to be more accentuated in September-October 1995 (Figure 2a) than in April-May 1996 (Figure 2b). A first conclusion for this comparison is that, globally, the directions of the currents are rather similar, with the same reverses along 7°30'N, but the magnitudes can be different (usually less for the altimetric current, rather affecting the meridional component).

Figure 3 gives a scatterplot of the ETAMBOT measurements versus TOPEX/POSEIDON deduced currents. For this purpose, both currents have been interpolated on the same geographical and temporal location. On average, the currents oscillate between +/-50 cm s^{-1} but can reach more. The symmetrical regression line [*Bauer et al.,* 1992]:

$$Y = 1.23867, X - 5.25609$$

is close to the "perfect" $Y = X$ case. Table 1 gives the average values and rms variabilities for each of the zonal and meridional components U and V, and for each of the ETAMBOT cruises and transects. The mean currents over the whole area are generally in agreement, both in magnitude and

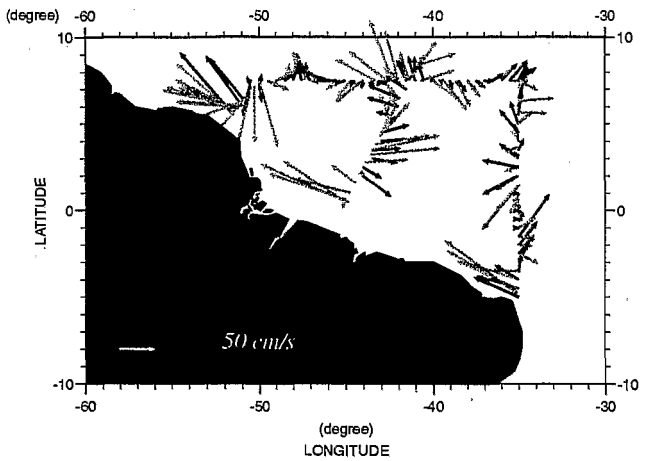

Figure 2a. Ship-mounted acoustic Doppler current profiler (SADCP) (shadded arrows) and altimetric currents (solid arrows) during ETAMBOT 1 in September-October 1995. Units are cm s^{-1}.

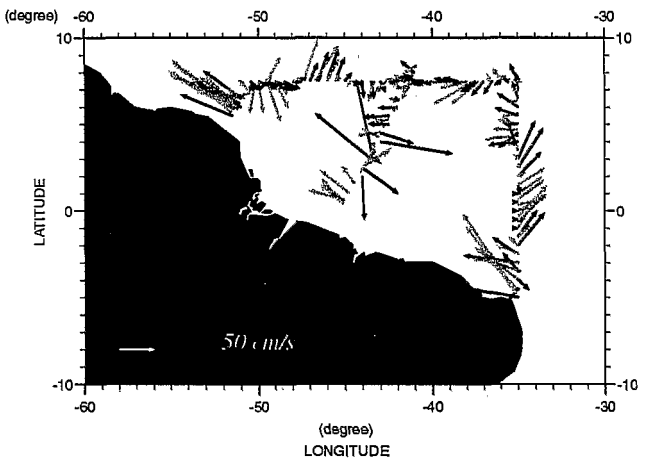

Figure 2b. Same as Figure 2a, except for ETAMBOT 2 cruise in April-May 1996.

direction. The ratio between the rms variabilities ranges between 0.9 and 1.4, and the rms differences are below the respective standard deviations except for the V component during ETAMBOT 2. Indeed, this rms difference is often larger for the meridional component than for the zonal component. This is due to the better meridional altimetric data coverage (along-track sampling is originally 7 km) than the latitudinal one (350-km spacing between adjacent tracks). The meridional gradient of SLA is therefore better resolved than the latitudinal one, and thus the U component of velocity is better estimated than the V component. Table 1 also confirms that the discrepancies between the currents are essentially a problem of magnitude of the respective components but not of sign. Along the 7°30'N transect, the mean currents are low, but the variability is high both for TOPEX/POSEIDON and the SADCP velocity and for both ETAMBOT 1 and 2. The TOPEX/POSEIDON variability is weaker than the SADCP variability. This is due to smoother meandering variability between 38°W and 50°W for TOPEX/POSEIDON than for the SADCP currents. Along 35°W, the comparison is better for U during ETAMBOT 1 and for V during ETAMBOT 2. This discrepancy for U is due to a northward extent of the altimetric NECC core compared to the SADCP current. The ratio between the variabilities still ranges between 0.8 and 1.3. Along the Ceara transect, we observe a stronger variability for TOPEX/POSEIDON than for the SADCP data during ETAMBOT 2. This is the worst result of the series and is due to the altimetric height problems along the American coast stated previously.

Looking more precisely at the surface current map, we notice a large anticyclonic feature off French Guiana (50°W, 5°N-7°N) in September-October 1995 (Figure 2a). West of 42°W, the meandering is so strong that the zonal component is alternatively eastward or westward. Strictly speaking, the eastward NECC appears during that period for both data sets only east of 42°W. This signature of the eastward NECC can also be seen from the SADCP current north of 5°N, along 35°W. However, the altimetric velocity is mostly northward there, with only a tiny eastward component. South of 5°N and down to 1°N, both currents are in good agreement and show westward direction (30-50 cm s^{-1}) associated with the South Equatorial Current (SEC) turning south when approaching the equator. Between 1°S and 3°S the currents are eastward. At the southernmost part of the 35°W transect, the currents reverse, again in agreement with the presence of the coastal and strong (75 to 100 cm s^{-1}) northwestward flowing NBC, which can also be observed in the southern part of the Ceara transect from the SADCP measurements. That part of the transect is too close to the coast and the equator, however, to allow reliable geostrophic calculations from SLA, so that we have no evidence here, from altimetry, of the coastal NBC. North of 2°N, along that Ceara transect, both currents are eastward, turning westward between 4°N and 5°N.

In April-May 1996 (Figure 2b) the currents are still in good agreement along 7°30'N. Contrary to September-October 1995, no anticyclonic NBC retroflection eddy is observed from both

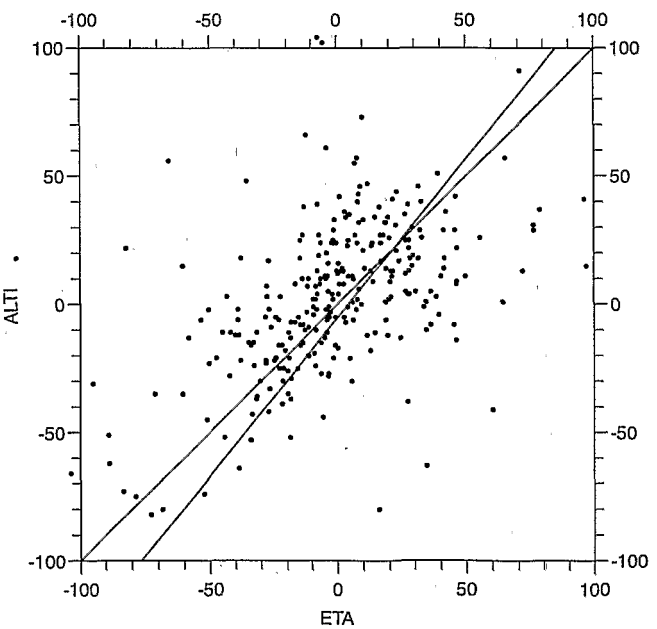

Figure 3. Scatterplot of ETAMBOT SADCP current measurements (ETA) versus TOPEX/POSEIDON deduced surface velocities (ALTI). Units are cm s^{-1}.

Table 1. Average Velocities for Zonal Component *U*, and Meridional Component *V*, and rms Variabilities for the Ship-Mounted ADCP (ETA) and TOPEX/POSEIDON (T/P) Deduced Surface Currents

	U		*V*		Var *U*			Var *V*			rms Difference	
	T/P	ETA	T/P	ETA	T/P	ETA	R	T/P	ETA	R	U	V
					ETAMBOT 1							
Global	-4	-2	14	4	29	38	1.3	25	36	1.4	26	36
7°30'N, 50°W-35°W	0	2	7	2	19	28	1.5	19	34	1.8	15	26
35°W, 7°30'N-5°S	-11	-9	21	5	32	42	1.3	25	23	0.9	25	25
Ceara	8	18	6	26	35	41	1.2	16	16	1.0	27	10
					ETAMBOT 2							
Global	-6	-14	8	5	33	30	0.9	29	27	0.9	27	35
7°30'N, 50°W-35°W	0	-7	-2	0	18	42	2.3	18	41	2.3	12	18
35°W, 7°30'N-5°S	-13	-23	17	15	34	29	0.8	26	25	1.0	24	5
Ceara	-2	-6	4	4	46	21	0.4	42	17	0.4	51	53

Units are centimeters per second. *R* means the ratio of the rms (ETA/TP). Values are presented for the global area, and for the three main transects sampled during the ETAMBOT 1 and 2 cruises.

currents around 50°W, off French Guiana. The eastward NECC is only suggested between 45°W and 50°W. A westward circulation is now observed in the eastern part of the transect, as along the northern part of the 35°W transect. Thus the NECC has totally disappeared from that transect in April-May 1996, and the SEC is observed farther north than in September-October 1995. South of 3°N, currents are eastward, before changing again westward south of 2°S, in agreement with the presence of the coastal NBC along the Ceara Rise. As already mentioned, the altimetric data are unrealistic between 1°N and 4°N during this cruise. However, north of this latitude, SADCP and altimetry agree again and show a weak and westward current.

We have checked if the differences observed in magnitude between the altimetric and the SADCP current could be due to ageostrophic components. First, we computed an Ekman drift from the ERS scatterometer wind product. We used the weekly 1° x 1° wind data sets from Centre ERS d'Archivage et de Traitement (CERSAT). For example, along 7°30'N during ETAMBOT 1, we obtain a mean zonal velocity equal to 0.3 cm s^{-1}, with a rms variability of 4 cm s^{-1}. For the meridional component we obtain a mean value of 6 cm s^{-1}. The rms variability is 4 cm s^{-1}. These values are clearly not enough to explain the discrepancies between the TOPEX/POSEIDON and SADCP values. Furthermore, the oscillations observed in the altimetric and SADCP currents along this latitude cannot be the result of relatively weak and steady trade winds in terms of Ekman drift.

As stated previously, the 7°30'N transect is a spawning area for meandering currents and mesoscale activity. Thus we have to check the influence of such mesoscale features on the results. If the horizontal scales of such disturbances are small enough, then the main balance issued from the Navier-Stokes equations is no more between the pressure gradient and the Coriolis forces (the geostrophic balance) than between the pressure gradient and the centrifugal forces. In that case, a better approximation to the actual flow than the geostrophic flow is given by the so-called "gradient wind" equation in meteorology [*Gill*, 1982]:

$$V = -fR/2 +/- (f^2R^2/4 - Rg\,\partial h/\partial n)^{1/2} \quad (2)$$

where *R* is the radius of the eddy structure. The gradient wind is the sum of the geostrophic and cyclostrophic components. Combined with (1), (2) can be rewritten as

$$V_g/V = 1 + V/fR \quad (3)$$

and gives the ratio between the geostrophic and the gradient flows. *Didden and Schott* [1993] found that most of the difference at 8°30'N,52°01'W between the amplitude of the fluctuations estimated from the Geosat altimeter and measured with a current meter was due to this cyclostrophic component. We did the same computations. In September-October 1995 we found, along 7°30'N, a ratio V_g/V ranging from 0.85 to 1.09. Thus considering the cyclostrophic component in that area would modify the results by around 10%.

Figure 4a and 4b show the monthly means of TOPEX/POSEIDON currents as observed in September 1995 and April 1996. We selected these two particular months as they are representative of the periods when the ETAMBOT cruises were carried on. The major features of incoming and outgoing surface flows, as hypothesized by *Bourlès et al.* [this issue] from analysis of water mass and SADCP measurements, are evidenced by altimetry. For example, in September 1995, an anticyclonic eddy develops at about 51°30'W,8°30'N (Figure 4a). It was surely its southern limit that has been sampled at 7°30'N during ETAMBOT 1. Figure 4a also emphasizes that current measurements made along a single section give only a partial view of the position and origin of a current such as the NECC: *Bourlès et al.* [this issue] locate the NECC origin between 45°W and 50°W in the 4°-8°N latitude range, i.e., south of the 7°30'N and north of the Ceara sections. It is shown here as a large NBC Retroflection pattern. At 50°W,10°N a southward flow, despite being close to the northern domain limit, could be the indication of a partial advection of North Equatorial Current (NEC) waters, which feed the NECC. *Bourlès et al.* [this issue] also mention that the southeastward surface flow observed along the Ceara transect around 5°N is fed by the NBC and then meanders eastward-

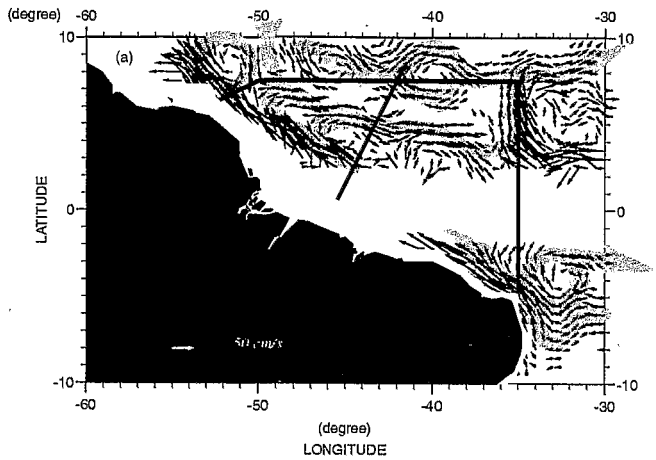

Figure 4a. Average current vectors for September 1995 obtained from TOPEX/POSEIDON. Units are cm s^{-1}. Mean flow trajectories are shaded. Only velocities over 10 cm s^{-1} are mapped.

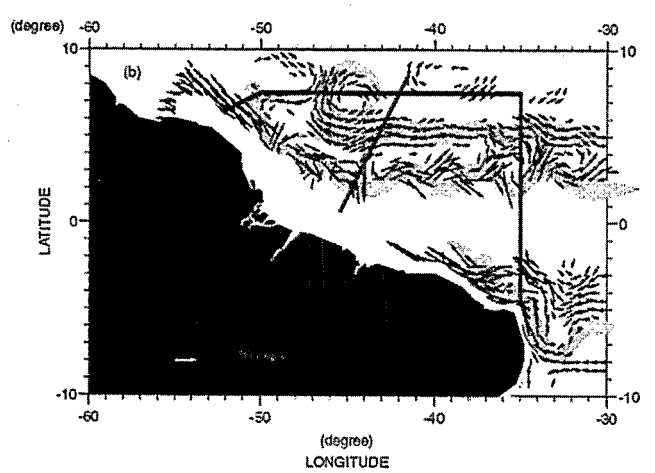

Figure 4b. Same as Figure 4a, except for April 1996.

northeastward to join the NECC at 35°W. This is clearly the pattern evidenced in Figure 4a, except that the northward flow at 35°W is intensified in the altimetric data compared to the SADCP currents. South of the equator, a northward current runs alongside the coast and joins the SEC to form the NBC at 35°W. Also interesting to note is a partial retroflection of the NBC south of the equator. *Schott et al.* [1998] and *Bourlès et al.* [this issue] observed a surface eastward jet above the EUC during different boreal fall cruises. Altimetric circulation seems therefore to indicate that part of the feeding of this equatorial eastward surface current is due to a partial retroflection of the NBC.

In April 1996 (Figure 4b), currents are globally weaker. Whereas a partial NBC retroflection is observed at 4°N,49°W, part of the NBC continues toward the Caribbean. In the same way, the NECC remnant along 7°30'N is only visible from 46°W to 50°W. The major currents are observed in the middle of the region, where an eastward meandering current centered on 4°N neighbors a westward meandering current centered on 5°N. Recirculations between the two opposite currents can be seen at 45°W and 35°W. South of the equator, the northward flowing coastal current merges with the SEC to form the NBC at 35°W, as in September 1995, but there is no more NBC Retroflection feeding a surface eastward current south of the equator.

3.3. Transport Variability

More than the currents by themselves, information on the oceanic transports is essential when looking at climate variability. Whereas hydrographic or ADCP measurements offer good vertical resolution but are sparse in time, altimetric data supply good temporal resolution but no information on the vertical. Thus, to attempt to obtain the transport time variability, the question is how to "project" the two-dimensioned (2-D) surface altimetric information in the vertical, at least in the upper layers. Past studies have shown that most of the temporal variability of the upper layer oceanic transport occurred in the first 100 m [*Garzoli*, 1992; *Johns et al.*, 1998], as the cores of the main surface currents are located in this layer. Thus we will consider the 0 to 100-m transports. The next purpose of this study is therefore to investigate how, when no in situ data are available, we can reliably obtain the temporal variability of the 0 to 100-m transports from altimetry only.

Similar extrapolation of the altimetric data to integrated transports has been conducted successfully in other parts of the ocean [*Garzoli and Gordon*, 1996; *Garzoli et al.*, 1997]. Usually, the authors face the problem of projecting, over the depth, the two-dimensional information given by altimetry by assuming either barotropy, statistical regression, or a linear (or exponential) decrease of the velocity with depth. *Carton and Katz* [1990] use a two-layer model to compute the NECC transport from Geosat sea level data. Also using Geosat data, *Goni et al.* [1996] propose a method to monitor the thickness of the upper layer and the barotropic and baroclinic transports in the Brazil-Malvinas Confluence region by using SLA and statistics. As shallow water models have proved to be quite efficient in the tropics to monitor upper layer dynamics (a key parameter in the tropics is the depth of the thermocline, which varies from 30-50 m in the east to 100-150 m in the west), we follow an approach similar to that of *Carton and Katz* [1990]. We assume that a baroclinic mode is dominant when looking at the 0- to 100-m transport variability in the tropical Atlantic, as it is for DH or current variability *[Du Penhoat and Treguier*, 1985; *Philander and Pacanowski*, 1986].

The vertical mode decomposition applied to the velocities gives

$$U(x,y,z,t) = \Sigma\, U_n(x,y,t)\, [\phi_n(z)]$$

for n=1,∞ the vertical mode number

$$V(x,y,z,t) = \Sigma\, V_n(x,y,t)\, [\phi_n(z)]$$

for n=1,∞

If a mode k is dominant, it follows that

$$U(x,y,z,t) \approx U_k(x,y,t)\, [\phi_k(z)]$$

$$V(x,y,z,t) \approx V_k(x,y,t)\, [\phi_k(z)]$$

and the local 0- to 100-m transport is

$$t_k(x,y,t) = \int_0^{100m} U(x,y,z,t)\, dz \approx \int_0^{100m} U_k(x,y,t)\, [\phi_k(z)\, dz]$$

or

$$t_k(x,y,t) = \int_0^{100m} V(x,y,z,t)\, dz \approx \int_0^{100m} V_k(x,y,t)\, [\phi_k(z)\, dz]$$

which can also be integrated over a direction α (α=x or y) perpendicular to the velocity to produce meridional or zonal transports

$$T_k(t) = \int_\alpha t_k(x,y,t)\, d\alpha$$

At the surface (obtained from altimetry)

$$U(x,y,0,t) \approx U_k(x,y,t)\, [\phi_k(0)] \Rightarrow U_k(x,y,t) \approx U(x,y,0,t)/\, \phi_k(0)$$

$$V(x,y,0,t) \approx V_k(x,y,t)\, [\phi_k(0)] \Rightarrow V_k(x,y,t) \approx V(x,y,0,t)/\, \phi_k(0)$$

and then,

$$T_k(t) = \int_\alpha t_k(x,y,t)\, d\alpha = \int_\alpha \int_0^{100m} U(x,y,z,t)\, dz\, d\alpha$$

$$\approx \int_\alpha \int_0^{100m} U_k(x,y,t)\, [\phi_k(z)]\, dz\, d\alpha$$

$$\approx \int_\alpha \int_0^{100m} U(x,y,0,t)\, [\phi_k(z)\, /\, \phi_k(0)]\, dz\, d\alpha$$

$$T_k(t) = \int_\alpha t_k(x,y,t)\, d\alpha = \int_\alpha \int_0^{100m} V(x,y,z,t)\, dz\, d\alpha$$

$$\approx \int_\alpha \int_0^{100m} V_k(x,y,t)\, [\phi_k(z)]\, dz\, d\alpha$$

$$\approx \int_\alpha \int_0^{100m} V(x,y,0,t)\, [\phi_k(z)\, /\, \phi_k(0)]\, dz\, d\alpha$$

The detailed procedure is the following. To check the method, "real" transports are first calculated from the SADCP data. We integrate the cross-section velocity over the upper 100-m layer, assuming a slab layer between 0 and 16 m where no data exist. These SADCP transports will constitute a reference basis to test the hypothesis we made to compute the altimetric transports. In a second step we use the hydrographic data to calculate vertical baroclinic modes over the area. We present only the results for the first two dominant baroclinic modes in the tropical Atlantic Ocean (ϕ_1 for the first mode (M_1) and ϕ_2 for the second mode (M_2)) [*Philander and Pacanowski*, 1986]. From the Brunt-Väïsälä frequency:

$$N^2_z = -g/\rho_0\, \partial\rho_\theta/\partial z,$$

where g = 9.8 m/s^2 is the acceleration of gravity, ρ_0 is the mean density value, ρ_θ is the potential density, and we obtain the vertical mode solutions ϕ_n of

$$1/N^2_z\, \partial^2\phi_n/\partial z^2 + \phi_n/c^2_n = 0$$

where c_n is the velocity associated with the mode n (n=1 or 2 as stated before). Plate 1 shows all the vertical profiles of ϕ_1 and ϕ_2 for the two cruises. The mean profile we used, calculated from all the profiles of both cruises, is also presented. As expected from previous studies, scattering of the individual profiles is prevalent in the upper layers, especially for the stations located close to the continental shelf. Both modes reveal a deeper mixed layer in boreal spring 1996 (about 150 m, Plates 1b and 1d) than in fall 1995 (about 50 m, Plate 1a and 1c). Upper layer values are also stronger in April 1996 than in September 1995. However, no seasonal surface variation can be seen for ϕ_1 between the respective characteristics of the different transects of the cruises (7°30'N, 35°W, Ceara, off French Guiana). The 7°30'N section always gives the highest values. This is not the case for ϕ_2, as the 7°30'N transect presents the highest values in boreal fall 1995, whereas the 35°W transect gives the highest values in boreal spring 1996. On the contrary, for the subthermocline layers (500-1000 m) the seasonal variations between the transects are mostly evidenced by ϕ_1. Therefore the seasonal variability is mostly associated with the second baroclinic mode for the upper oceanic layers and with the first baroclinic mode for the subthermocline layers. The mean profile obtained from these data presents a 150-m mixed layer depth for ϕ_1 and a first zero crossing around 200 m for ϕ_2. We will check later on the resulting influence of the variability we neglected using this mean profile in the calculations. After having obtained the mean profiles ϕ_1 and ϕ_2, we are able to get, from the altimetric velocity U_{alt}, V_{alt}, the vertical cross-section transport approximation over the first 100 m depth as described previously.

Plate 2 gives an example of the calculations along 7°30'N for both cruises. It shows the meridional transport calculated over the first 100 m depth and between each station pair of the transect, as given by altimetry for M_1 or M_2 or by SADCP. The agreement is rather good for both cruises. The transports are mostly northward, especially in September 1995, and vary from -3 to +4 Sv (1 Sv = 1.10^6 m^3 s^{-1}). It is impossible to distinguish any significant difference between the altimetric transport computed either with the first mode or with the second one. The rms differences between the altimetric and the SADCP transports equal 0.89 Sv in September 1995 and 0.87 Sv in April 1996. This is below the errors induced on the transports by the velocity errors themselves (around 0.3 Sv for the SADCP transports and 0.9 Sv for altimetry at this latitude). To check the efficiency of the method, which consists of using a mean baroclinic mode to get information in the vertical from altimetry, we also use the surface SADCP current and the same mean baroclinic mode profiles to estimate transports in the same way as the "altimetric" ones. The results are also shown in Plate 2. Apart from a slight discrepancy occurring during ETAMBOT 1 between 37°W and 39°W, the three curves ("real" SADCP transport, "M_1" SADCP transport, "M_2" SADCP transport) are nearly indistinguishable. This result obtained with the SADCP data also comfirms our choice of the mean profile. If this profile was inappropriate, then discrepancies between "real" and "approximated" transports would result. To check it, we recompute the transports by using two profiles that are on the opposite edges of the vertical mode variability (Plate 1). The results (not shown), in terms of transports, do not reveal significant differences, with all the values differing by less than 5%. The method therefore seems robust for the upper layer transport computation, and the differences observed between altimetric and SADCP transports are mostly due to differences in surface velocities as noted before.

The agreement found between in situ measurements sampled during boreal fall 1995 and spring 1996 and the TOPEX/POSEIDON data in terms of SLA, surface velocities, and upper layer transports inclined us to study the spatial and temporal variability over the ETAMBOT area between 1992 and 1997 from altimetry.

4. Tropical Atlantic Western Boundary Variability Between 1992 and 1997

4.1. SLA Variability

We approach the temporal variability of the SLA over the ETAMBOT area using an empirical orthogonal function (EOF) analysis, which has proved to be a very powerful tool for

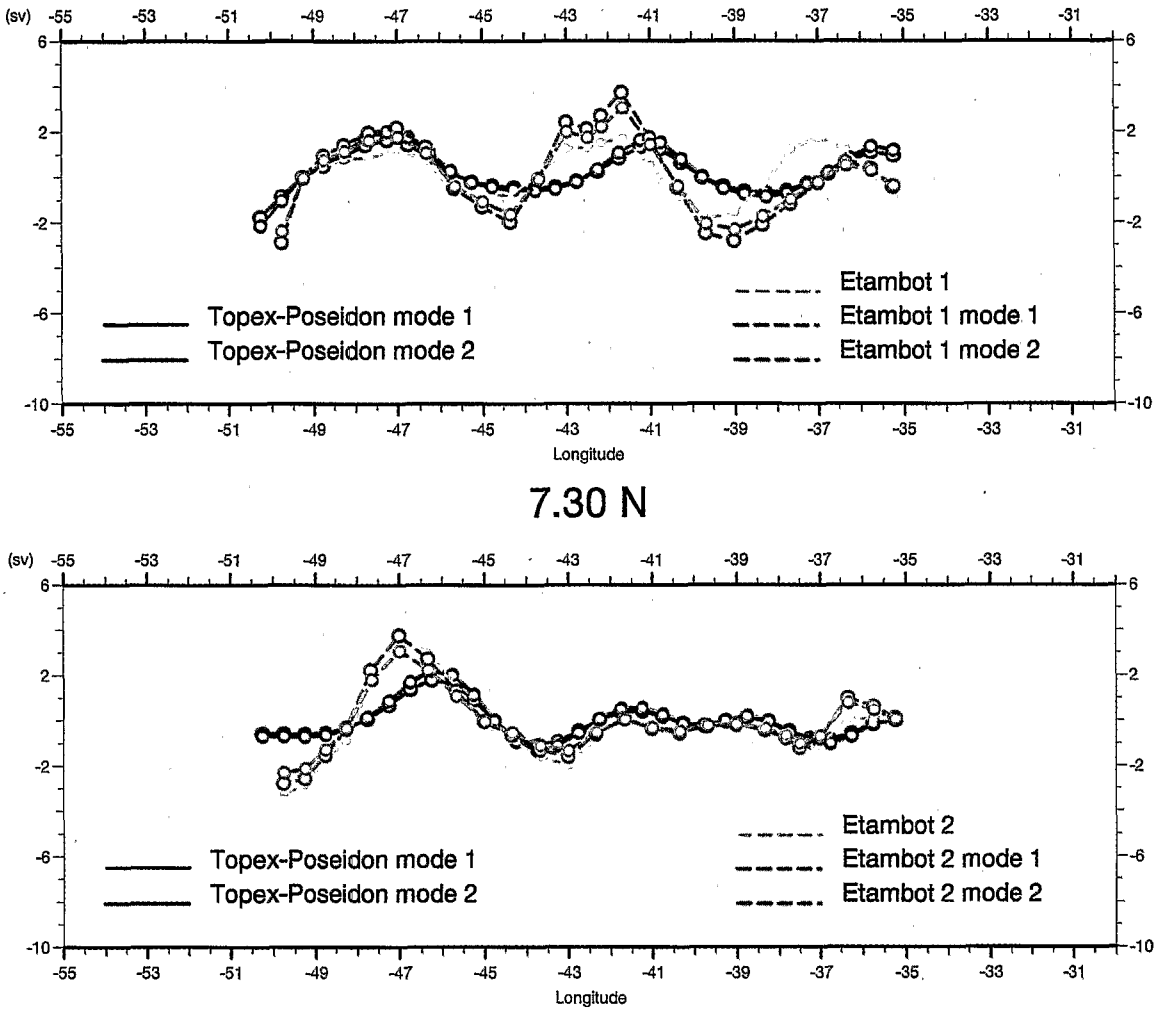

Plate 2. Meridional transport integrated over the first 100 m depth and between each station pair of the 7°30'N transect as given by projecting altimetry over a first baroclinic vertical mode profile (solid black line), a second baroclinic vertical mode (solid, dark blue line), or by SADCP (dashed yellow line). For reference, the transports obtained by projecting the SADCP surface data on the first baroclinic vertical mode profile (dashed, light blue line) or a second baroclinic vertical mode (dashed pink line) are also displayed. Units are sverdrup (10^6 m^3 s^{-1}). The barycenter of each station pair used to compute the transport is indicated by a circle. The total meridional transport integrated along 7°30'N from 35°W to 50°W can be obtained by adding these discrete values (For example, this gives, during ETAMBOT 1, around 6 Sv for the SADCP and 8.5 Sv for altimetry projected over the first mode).

isolating and understanding physical processes in oceanography and meteorology [*Lorentz*, 1969; *Davis*, 1976] (a review of the problem is given by *Von Storch and Navarra* [1993]). We first analyzed the 5-day time series over the nearly 5-year period. From a mathematical point of view, this means that we considered detrended row vectors of ≈365 points length (5-day resolution ≈ 73 points per year x 5 years) in the matrix, of which the covariance has to be computed to solve the eigenvalue problem. As expected from previous studies [*Duchêne and Frankignoul*, 1991; *Arnault and Cheney*, 1994], the first functions present clearly annual signals (12-month, 6-month, and 2- to 3-month periods), with slight year-to-year ("interannual" in the following) variability. Thus we reanalyzed these results, focusing first on a mean annual signal, then on the interannual deviation. We have decomposed the EOF annual signal into an intraseasonal and an annual study. Thus the matrix considered for the intraseasonal variability uses 5 years of 3-month realization with a 5-day resolution (20 realizations). It has detrended row vectors of ≈ 18 points. The matrix for the annual study uses 5 years of 12-month realization with a 5-day resolution (five realizations). It has detrended row vectors of ≈73 points. The interannual deviation has been computed then by subtracting the annual mean. The EOF interannual analysis is performed on a matrix of 365 point row vectors (5 years with a 5-day resolution). Table 2 gives the variances and the percentages of variance explained by each of the first five EOFs computed for these periods.

4.1.1. Intraseasonal variability. As shown in Table 2, the first two EOFs explain more than 60% of the intraseasonal variance. Figure 5 presents the spatial and temporal structures associated with these two EOFs. Both show an area of extrema located between 3°N and 8°N. A zonal succession of highs and lows appears with a horizontal scale around 400-600 km, reduced westward. It is close to the scale of the meanders observed during the cruises at 7°30'N. The temporal structures are nearly sinusoidal with a 2- to 3-month period. Lag correlations indicate that these two EOFs are representative of the same dynamics, the westward propagation of a wave-like structure along these latitudes. Common EOFs are not suitable for representing propagating features, which will appear "split" over several functions as shown in Figure 5; but these propagations, starting between 30°W and 35°W, are evident throughout the 1992-1997 years on a SLA longitude versus time diagram at 7°30'N (Figure 6). The mean propagation speed is about 13 cm s^{-1}, which is consistent with the characteristics of the first baroclinic mode Rossby waves off the equator. Many authors have investigated these features in recent years [*Johns et al.*, 1990; *McClean and Klinck*, 1995]. This point will be reconsidered in the following sections.

4.1.2. Annual variability. Diagnostics have been obtained from past studies on the seasonal cycle of the tropical Atlantic surface layer dynamics. For example, on a global scale and with a coarse resolution, *Merle and Arnault* [1985] and *Duchêne and Frankignoul* [1991] analyze the seasonal cycle of the dynamic topography from hydrographic data. *Richardson and McKee* [1984] study the variability of the surface circulation from ship drifts. These studies were pursued with the first altimetric missions GEOS, Seasat, and Geosat [*Ménard*, 1988; *Carton*, 1989; *Arnault and Cheney*, 1994]. The NECC region and the western boundary annual signal characteristics were also investigated from either in situ or satellite data [*Carton and Katz*, 1990; *Didden and Schott*, 1992; *Garzoli*, 1992]. All these results emphasize the strong influence of the seasonal cycle in the tropical Atlantic variability. This is also evident from Table 2 when looking at the variance of seasonal variability compared with those of the other timescales. We do not offer here another exhaustive description of the well-known features of the tropical Atlantic SLA seasonal cycle. As seen from Figure 7, most (60%) of the variability is due to a seasonal contrast between boreal winter-spring and boreal summer-fall situations (Figure 7a). The geographical area involved in this 12-month variability is shown as a large east-to-west tongue located between 2°N and 6°N, extending northwestward when reaching the American coast. This is the well-known signature of the NECC high, maximum in boreal summer-fall, and of the NBC signal along the coast. A change in sign is clearly evidenced at about 6°N, shifting northward in the eastern part of the domain. The second and third EOFs (12% and 7%, Figures 7b and 7c) represent a lower-period variability (6 months) and involve geographical areas located northward and southward of the NECC high: 6°-10°N for the strongest part and then 2°N-2°S for the weakest. As recalled by *Garzoli* [1992], from a statistical point of view, this must be so because the percentage of the variance explained by the sum of all modes has to be equal to 100%. Therefore modes 2 and 3 must show higher amplitude at those locations where mode 1 amplitudes are lower. From an ocean dynamics point of view, the sea level deepens twice a year, in December-January and then July, north of 6°N (Figure 7b).

The annual variation depicted by this analysis reflects the response of the ocean through Ekman pumping to wind forcing

Table 2. Variance and Percentage of Variance Explained by First Five Empirical Orthogonal Functions Computed From TOPEX/POSEIDON Sea Level Anomalies for the Intraseasonal, Annual and Interannual Signals

	Intraseasonal			Annual			Interannual		
	Variance	% Var.	%Total	Variance	% Var.	%Total	Variance	% Var.	%Total
EOF 1	183	34	34	9560	60	60	1822	23	23
EOF 2	145	27	62	1994	12	72	1066	14	37
EOF 3	64	12	74	1127	7	79	647	8	45
EOF 4	52	10	84	599	4	83	560	7	52
EOF 5	24	4	88	517	3	86	491	6	59

Variance are in cm^2 integrated over the region: 1143 data points.

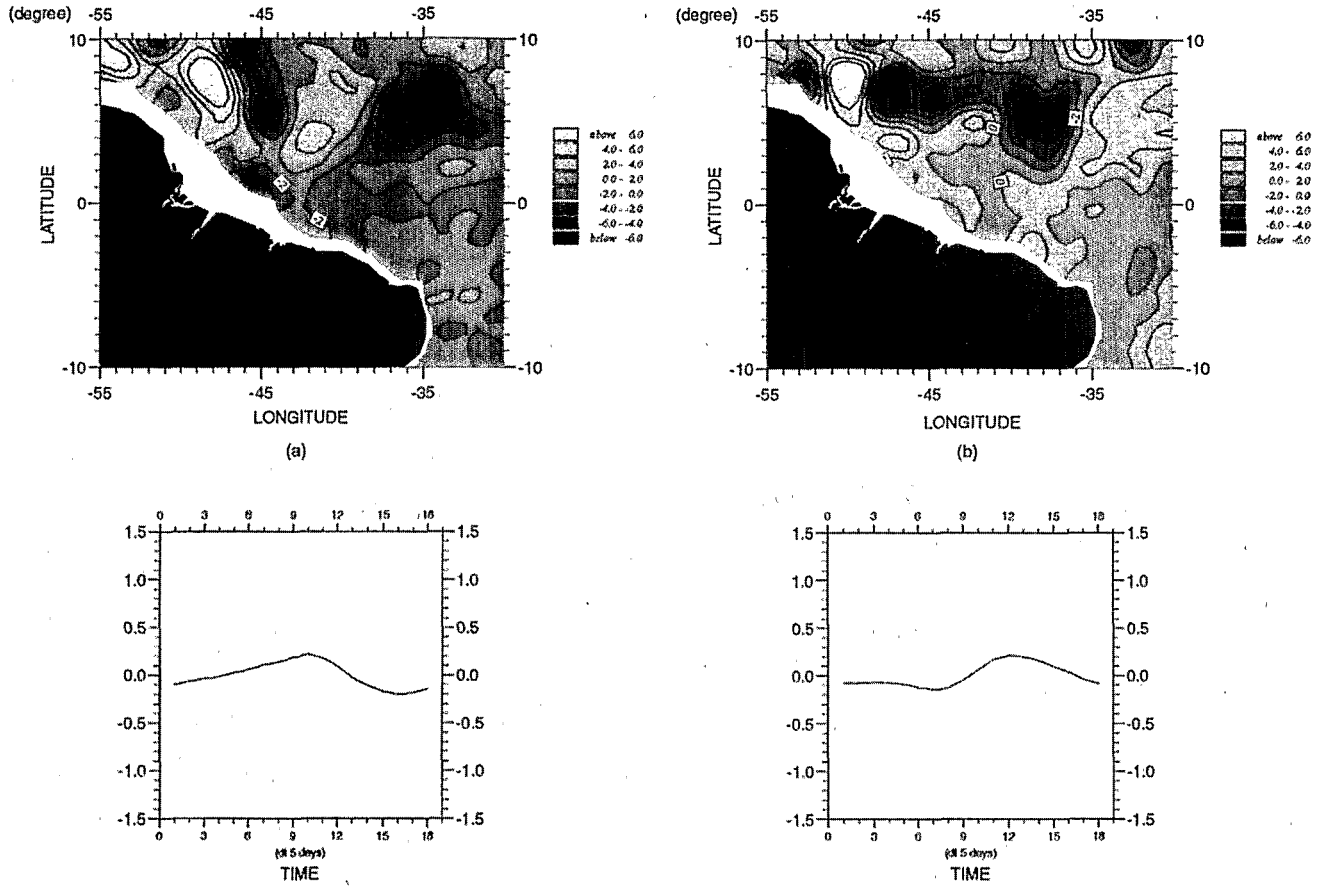

Figure 5. Time series (over a mean quarter) and spatial structures (in centimeters) associated with (a) the first and (b) second orthogonal functions for the TOPEX/POSEIDON SLA intraseasonal variability. Time step for the time series X axis is 5 days.

and the Intertropical Convergence Zone (ITCZ) north-south migration, as the dynamics of the NECC is directly related to the wind stress curl and its zero line and latitudinal location [*Garzoli and Richardson*, 1989].

4.1.3. Interannual variability. As stated previously, the annual cycle is the dominant signal in the tropical Atlantic Ocean, contrary to the Pacific Ocean. However, interannual variability (or at least "year-to-year" variations) has been detected. *Philander* [1986] reports the abnormal conditions observed during the FOCAL/SEQUAL program in 1984. *Katz* [1993] analyzes the NECC variability between 1983 and 1989 from inverted echo sounders (IESs) and finds a subsequent interannual variability in the NECC transport. *Arnault and Cheney* [1994] find, with Geosat data, an "El Niño like" event occurring in the tropical Atlantic basin in 1987-1988, which affects the mass transport between equatorial and extraequatorial areas.

Figure 8 shows the characteristics of the first EOF referring to these long periods. As the annual cycle observed from these 1992-1997 years is realistic and in agreement with previous studies, it is meaningful to discuss the anomalies from this annual cycle. This first EOF (23%) indicates that in a large part of the geographical area (35°W-45°W x 0°N-10°N) the SLA varies in phase. Besides 2- to 4-month fluctuations, the SLA decreases from November 1992 until January 1995, then a rapid inversion of the tendency occurs until the end of 1995, preceding a new decrease until June 1996, when a new inversion starts, lasting until May-June 1997. As a first approach, assuming that the SLA variations are mostly due to steric effects, a SLA decrease would reflect the incoming relatively cold and/or salty waters. On the contrary, a SLA increase expresses the presence of warm and/or fresh waters. Thus Figure 8 indicates that from November 1992 until January 1995, the region became relatively cold and/or salty, then a warm (fresh) event occurred in 1995, peaking in November, before returning to a colder/salty situation, peaking in June 1996, and finally, a new warming (refreshment) developed from mid-1996 until the end of the series in boreal summer 1997. Apparent in Figure 8 is that boreal winter 1994-1995 was the "coldest" period, while boreal spring-summer 1997 was the warmest one. It is interesting to note that the September-October 1995 cruise was conducted when one of the warm/fresh tropical Atlantic events was fully developed, contrary to the April-May 1996 one, which took place during a colder/saltier situation as shown in Figure 8.

4.2. Surface Current Variability

During the National Oceanic and Atmospheric Administration (NOAA) Subtropical Atlantic Climates Studies (STACS 11) experiment, a current meter mooring (S3) was located at 5°17'N,46°48'W [*Johns et al.*, 1998]. As a first look at the altimetric surface current variability, Figure 9 reproduces

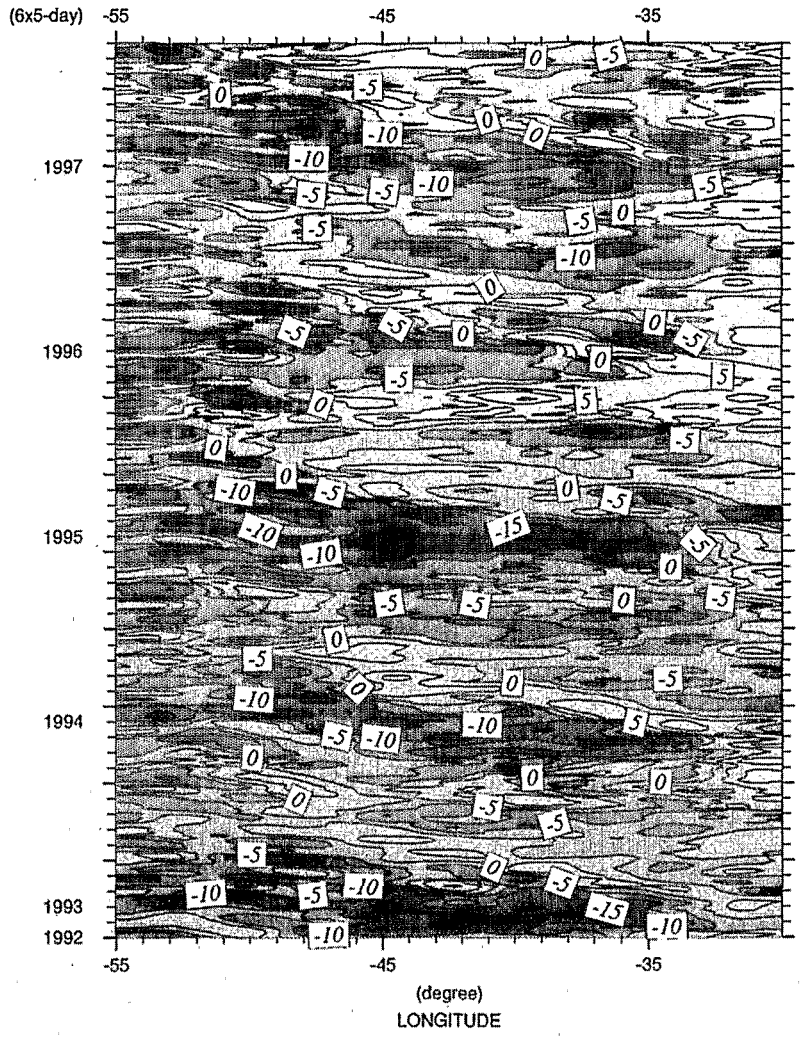

Figure 6. Time versus longitude plot of TOPEX/POSEIDON SLA along 7°30'N from November 1992 until August 1997 and from 30°W to 55°W. Time step is 5 days. Units are cm. Dark shading is for negative values; light shading is for positive ones.

the currents obtained at 160 m by this mooring [*Johns et al.*, 1998, Figure 2a] along with a vector time series of the "altimetric" current at the same location. *Johns et al.* [1998] notice that the near-surface current meter shows prominent reversals on relatively long timescales and appears to be seaward of the influence of the mean NBC boundary flow regime. *Johns et al.* [1998] find a mean southeastward and weak current of 12 cm s^{-1}. While they do not have any data available in the upper 100 m at this site, they assume that this offshore reversal reflects the return flow of the NBC Retroflection and that the surface currents at this site would have a similar mean direction. They also remark that the flow reverses from weakly northward or northwestward in boreal spring to southeastward in boreal fall, which is consistent with the expected development of the NBC Retroflection during this period. This variation is in excellent agreement with the altimetric currents shown in Figure 9. The series is longer than their current meter measurements, extending over 58 months (November 1992 to August 1997) instead of 15 (September 1989 to January 1991), and every year, the southeastward flow in boreal fall is evidenced from altimetric data. The mean flow computed over the entire series is effectively southeastward and weak, 10 cm s^{-1}. The year-to-year variation at this location is also weak: the mean flows computed for the three September-to-January (in concordance with *Johns et al.* [1998]) periods of the series range between 8 and 12 cm s^{-1}, all southeastward.

The mean power spectrum computed for the zonal and meridional velocity component time series along 5°N is given in Figure 10. The spectrum is red for frequencies down to around 1/100 days. A first peak is centered at 63 days, for both the zonal and meridional component. It corresponds to the intraseasonal variability observed in the SLA. *Johns et al.* [1990] have observed oscillations with a mean periodicity of about 50 days from current meter moorings in the western tropical Atlantic. These authors suggest that the oscillations arose from a single, coherent wave process. They speculate that they could be associated with the shedding of NBC Retroflection eddies. However, *Didden and Schott* [1993] compare the occurrences of Geosat altimetric eddies with the

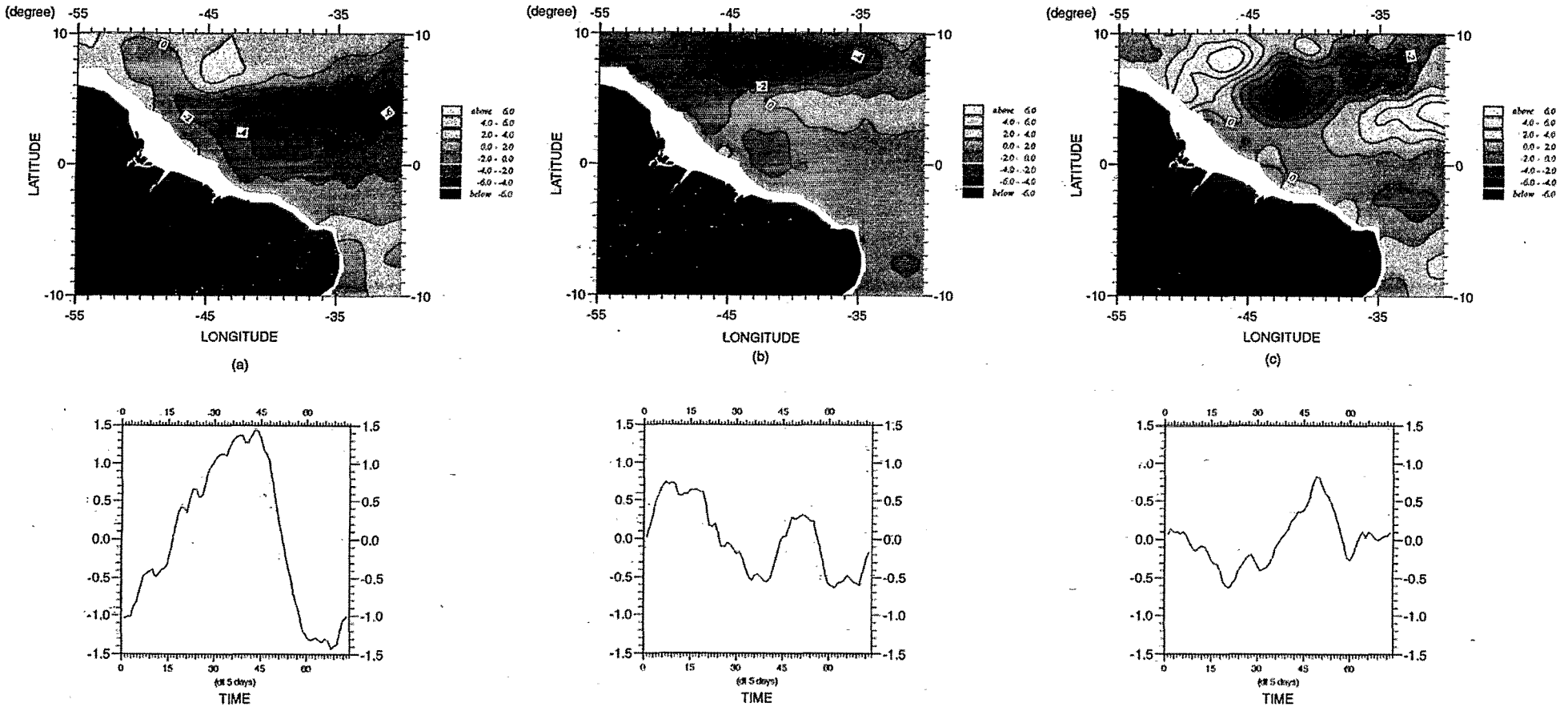

Figure 7. Time series (over a mean year) and spatial structures (in centimeters) associated with (a) the first, (b) second, and (c) third orthogonal functions for the TOPEX/POSEIDON SLA seasonal variability. Time step for the time series X axis is 5 days, starting in November. With this 5-day resolution a month is approximately equivalent to six ticks. For example, June begins at 43 and ends at 49 on the X axis; September corresponds to X values between 61 and 67.

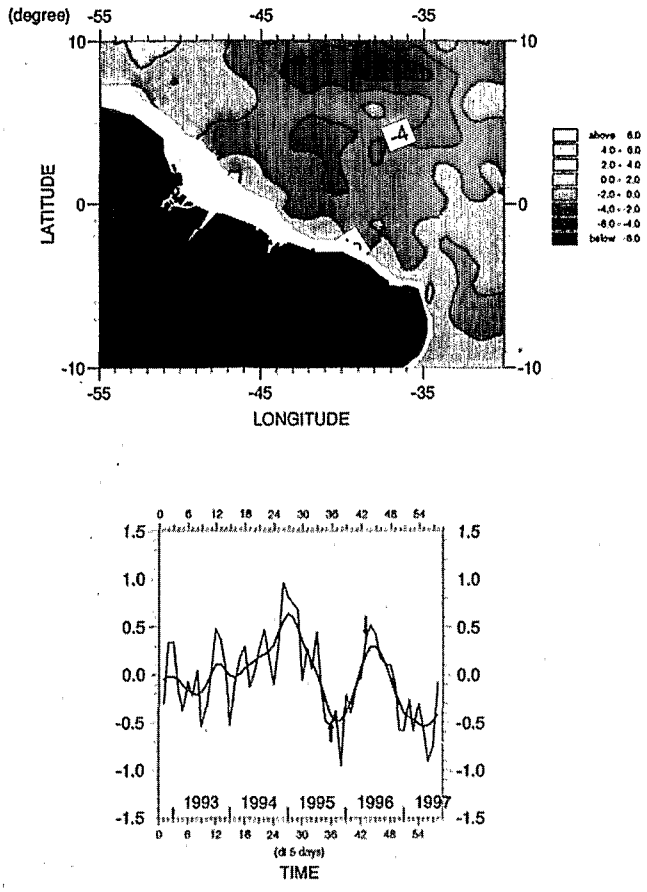

Figure 8. Time series (over the 5 years) and spatial structures (in centimeters) associated with the first orthogonal function for the TOPEX/POSEIDON SLA interannual 1992-1997 variability. Time step for the time series X axis is 1 month, starting in November 1992 and ending in August 1997 (X values from 1 to 58). ETAMBOT 1 was conducted during September-October 1995, months 35-36 on the X axis, and ETAMBOT 2 was conducted during April-May 1996, months 42-43. Arrows indicate these two cruises. Dashed curve is for the rough signal, and solid curve is for a low-pass filter of this signal (obtained with a Hanning 4-month filter to display large temporal scale tendency).

same current meter series and find that although the oscillations persist throughout 1987-1988 in the current measurement near the retroflection zone, only those of boreal winter are associated with eddies identifiable in the altimetric maps. *McClean and Klinck* [1995] try to analyze the dynamics of these oscillations from the results of the WOCE Community Modeling Effort (CME). They suggest that the 50-day oscillations are due to Rossby waves produced by the NBC Retroflection. These Rossby waves have very slow eastward group velocity and are advected eastward by the NECC until they reach 35°W, where they dissipate. A standing wave pattern is established for several months, while the NECC is active. Once it weakens, the waves are advected westward and disappear totally by May. However, according to *Johns et al.* [1998], the source of energy for these 40- to 60-day frequency fluctuations and eddies forming in the NBC Retroflection zone is not yet clear. It could be the scenario proposed by *McClean and Klinck* [1995], the northward propagation of an eddy-like feature along the coast from the equatorial region [*Carton*, 1991], or a local instability of the NBC. They conclude that analysis of satellite observations may be able to shed further light on these dynamics. We will not discuss further these 40- to 60-day oscillations in the tropical Atlantic as seen from TOPEX/POSEIDON altimetry, as they constitute a separate paper; but, once again, we can state that despite the coarse resolution of the TOPEX/POSEIDON altimetric mission dedicated to large-scale processes, mesoscale variability is also evidenced by the data. Thus interesting investigations, as suggested by *Johns et al.* [1998], could be carried out on this topic with such a satellite tool.

In Figure 10 the 5°N spectrum is white for the long periods with energy peaks at about 110-120 days, then 180-200 days, and 360 days. Figure 10 also reveals that the large-scale temporal fluctuations (over 300 days) of currents at 5°N are mostly zonal. The annual peak (360 days) is nearly twice as energetic for the zonal component as for the meridional one. This tendency is maintained for the longer periods. A slight peak is visible for the zonal velocity around 900 days and not for the meridional, but this result must be considered with caution because with a 5-year time series, a 900-day period is not really well resolved.

4.3. Transport Variability

Garzoli [1992] and *Katz* [1993] use IESs moored along 38°W (0°N, 3°N, 6°N, and 9°N) together with numerical models to compute the NECC transport. We used the same meridional transect, 38°W, and the same latitudinal extents (3°N-9°N) to compute the transport from the altimetric measurements in the upper 100 m as explained in section 3.3. Figures 11a-11d present this transport across 38°W. The global transport between 3°N and 9°N (Figure 11a) shows a regular seasonal oscillation, in agreement with previous studies. The transport is maximum eastward in the boreal summer-fall season (10 Sv in a mean) and minimal and even westward in boreal spring (-5 Sv). Splitting the latitudinal extent into two areas (6°N-9°N then 3°N-6°N; Figures 11b and 11c) reveals that most of the variability occurs in the southern area. The northern one exhibits more chaotic features, especially during the last 2 years, 1996 and 1997. Year-to-year variations are also clearly evidenced in Figure 11a. The eastward transport loses about 35% of its strength during the second half of 1995 compared with 1994. This event is followed by a stronger than usual westward transport in early 1996. This is when the ETAMBOT cruises were conducted. Then, in boreal fall 1996 the situation returns to "normal," but in early 1997 the transport seems unusually eastward. Looking at Figures 11b and 11c, it is clear that the weak eastward transport measured in boreal fall 1995 is mostly due to a weak 6°N-9°N eastward contribution. This confirms the observation we made with the SLA EOF analysis, when the interannual variability was mostly concentrated between 6°N and 9°N.

Finally, Figure 11d shows the meridional volume transport across the 7°30'N ETAMBOT transect, integrated between 50°W and 35°W. The transport is northward during the whole period. A seasonal cycle can be detected with maximum transport during boreal winter and minimum in spring; but what is particularly obvious in Figure 11d is the interannual variability that is shown with an increasing tendency of the northward transport starting from the lowest value (3 Sv) in April 1993 until boreal fall 1995, where the maximum value for the period (20 Sv) is reached.

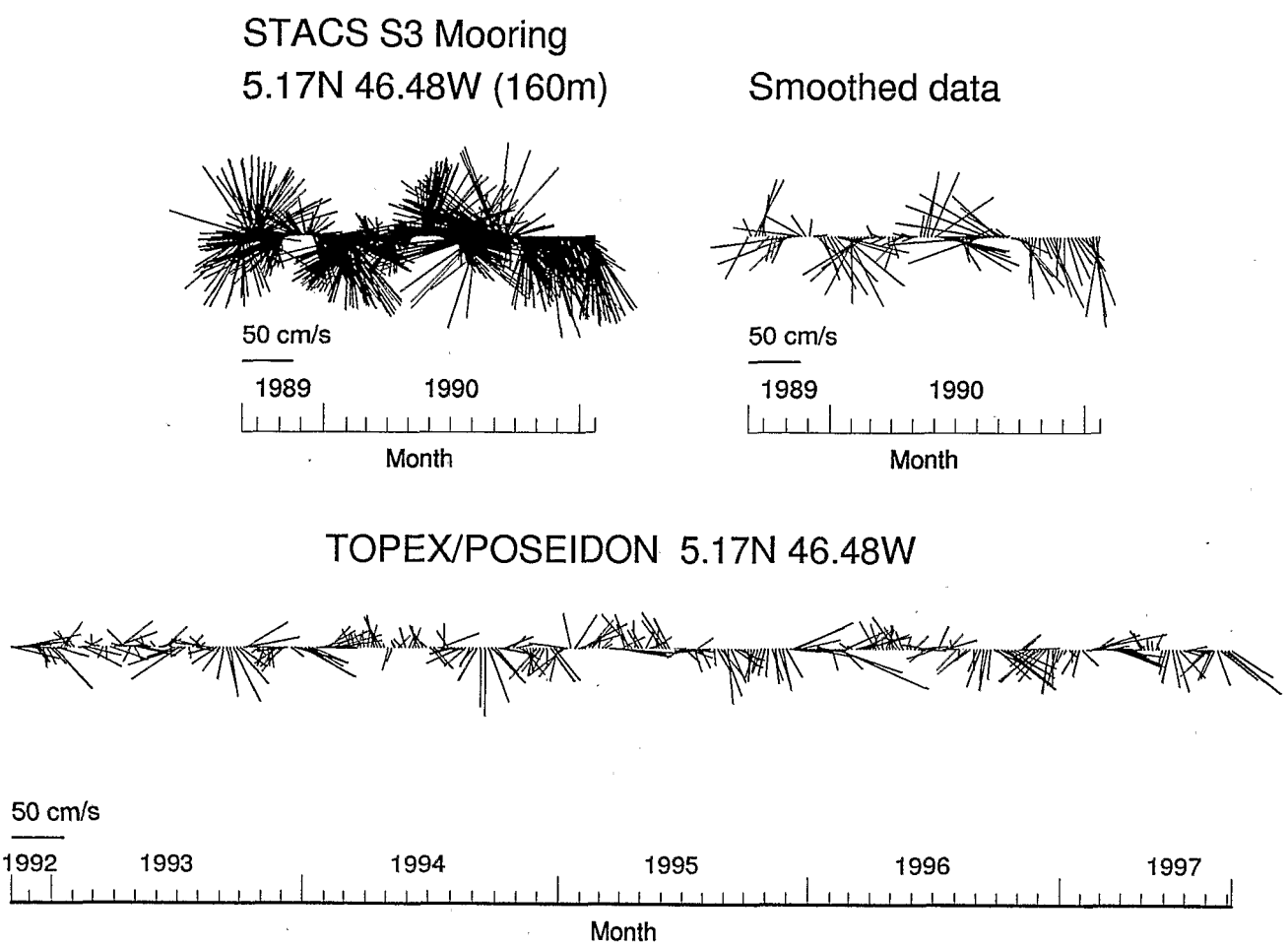

Figure 9. (top) Vector time series from September 1989 until January 1991 of the Subtropical Atlantic Climate Studies (STACS) mooring at 5°17N, 46°48W (courtesy of W.E. John and R.J. Zantopp). The current meter is at a 160 m-depth. Unit is cm s^{-1}. (Left) Raw data (twice a day) and (right) smoothed data averaged over 10 days with a 5-day sampling. (bottom) Vector time series from November 1992 until August 1997 of the altimetric surface current at 5°17N, 46°48W. Unit is cm s^{-1}. This location has been selected to be compared with site S3 of the STACS11 experiment.

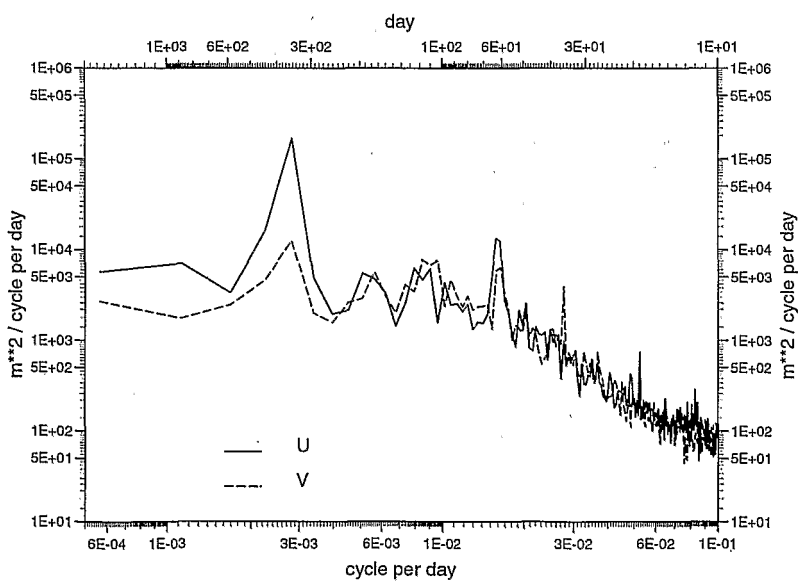

Figure 10. Mean temporal power spectrum along 5°N of the zonal velocity (solid curve) or meridional velocity (dashed curve) as computed from TOPEX/POSEIDON data.

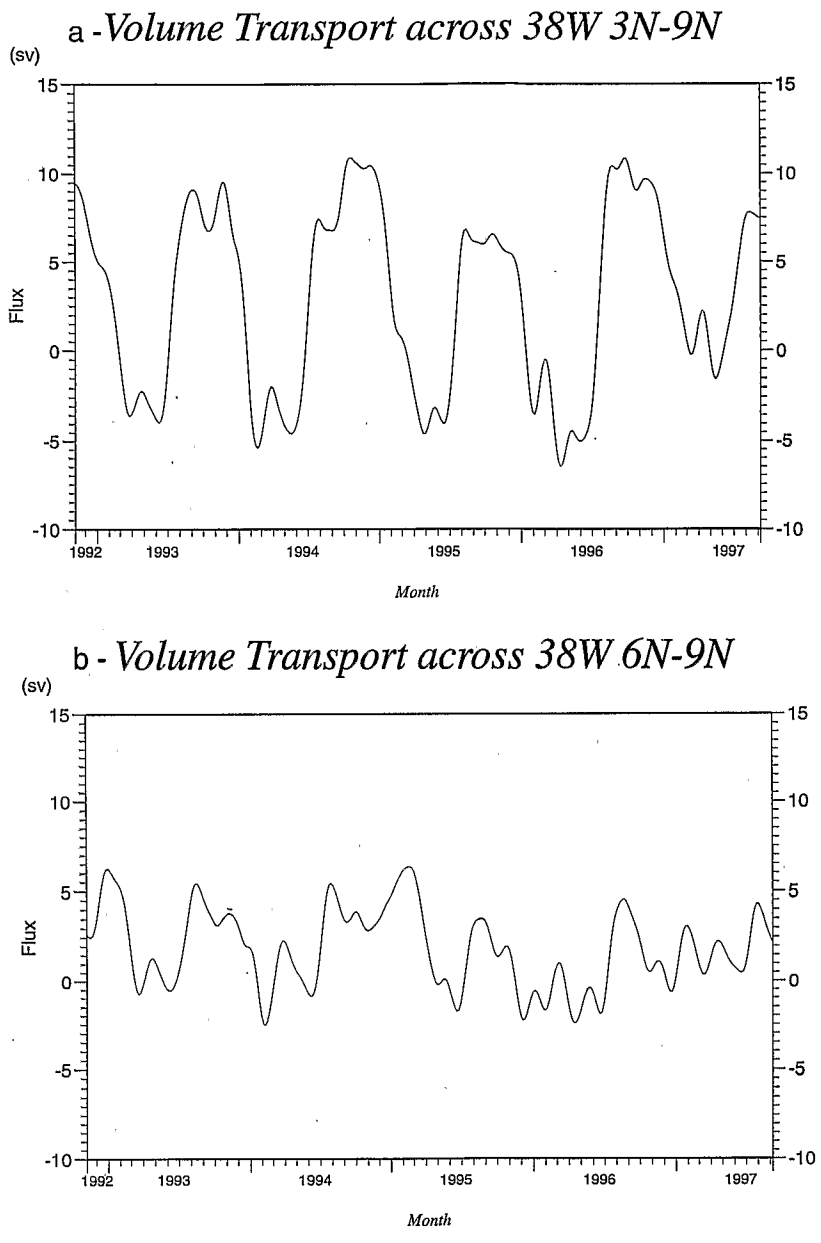

Figure 11. Upper layer volume transport (in Sverdrups, where 1 Sv = 10^6 m^3 s^{-1}) across 38°W and (a) between 3°N and 9°N, (b) 6°N and 9°N, (c) 3°N and 6°N, and (d) across 7°30'N between 50°W and 35°W.

5. Summary and Conclusion

Previous investigations based on in situ observations [*Johns et al.*, 1990; 1998; *Garzoli*, 1992; *Bourlès et al.*, 1999, this issue] detail the circulation scheme in the western tropical Atlantic. The problem is to determine whether or not a cruise is representative of a "mean" situation in space and time. Other studies based either on satellite data or model results [*Carton and Katz*, 1990; *Didden and Schott*, 1992, 1993; *McClean and Klinck*, 1995] shed light in a more general context; but past satellite missions are of short duration and not accurate enough to resolve the appropriate scales of the western boundary dynamics (from 100 to 1000 km lengths and from intraseasonal to interannual time periods), and models are sensitive to inaccuracies in surface forcings and parameterization.

Thanks to the long duration of the TOPEX/POSEIDON mission and the high level of accuracy of the altimetric data, we have been able to describe fully the variability of the SLA in the western tropical Atlantic from 1992 until 1997. With the data sets sampled during the ETAMBOT cruises in boreal fall 1995 and spring 1996, a new approach to determine surface current variability together with volume transports has also been reached.

First, the intercomparison between SLA and ETAMBOT DHA along the different sections of the cruises is good. The large-scale slopes given by the in situ measurements are well reproduced by altimetry; but even more encouraging for the TOPEX/POSEIDON mission is that mesoscale activity is also detected by the satellite data through use of an objective analysis. The mean rms difference over all the cruises between SLA and DHA is below 3 cm, while typical changes over the geographical area range from 10-20 cm.

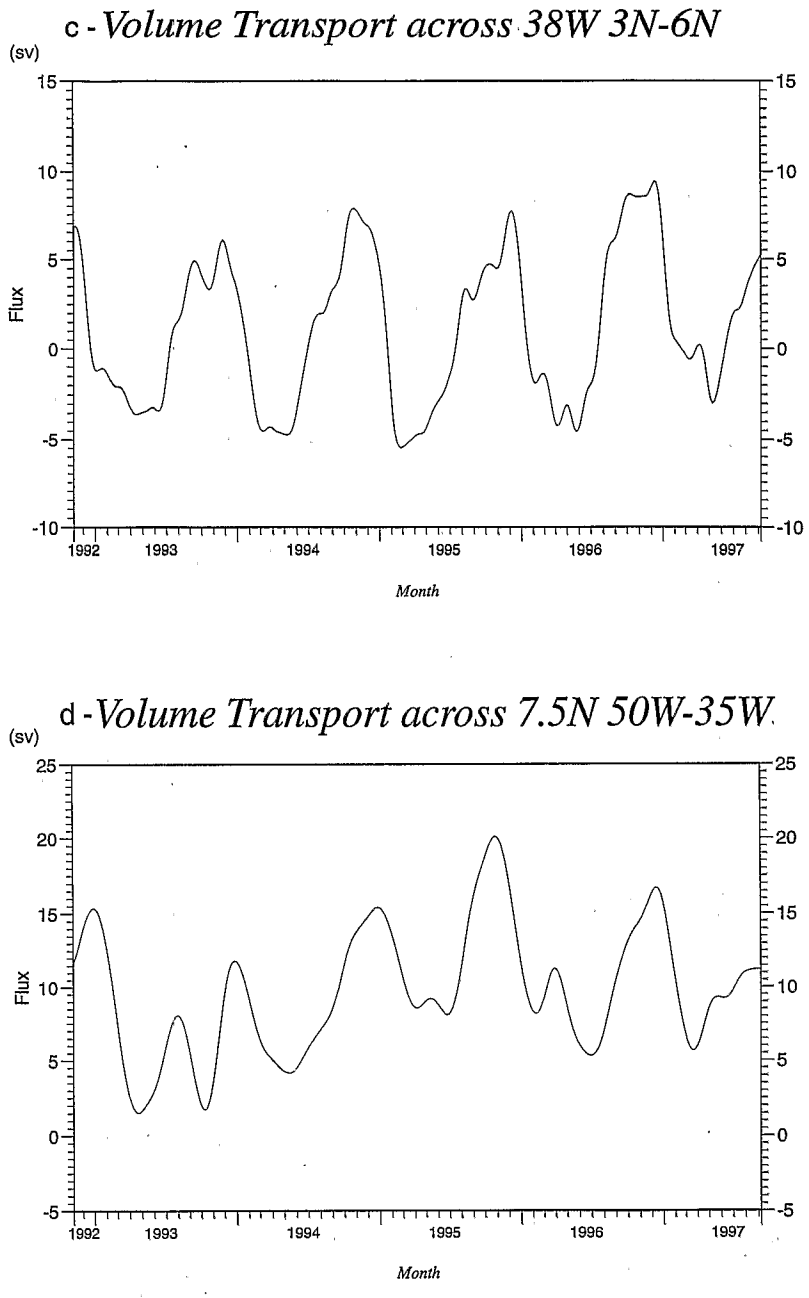

Figure 11. (continued)

In term of surface currents, off the equatorial band 2°N-2°S, the agreement between altimetry and SADCP data is qualitatively good. Most of the meandering and eddy-like structures evidenced during the cruises are also revealed on altimetric maps. During boreal fall 1995 and spring 1996, both currents present nearly the same spatial extent, the same reversal. The discrepancies in terms of magnitude are mostly due to the coarse latitudinal TOPEX/POSEIDON resolution, which affects the meridional velocity.

Assuming that the upper layer transport variability in the western tropical Atlantic is mostly baroclinic at the first order, we transform the altimetric surface current into upper layer volume transport, using the vertical modes obtained from the in situ measurements. We test the hypothesis by comparison with the SADCP transports computed over the upper 100-m layer. The rms differences between the altimetric and SADCP transports are around 0.9 Sv during both cruises.

This agreement between in situ measurements and TOPEX/POSEIDON data during boreal fall 1995 and spring 1996, in terms of SLA, surface currents, and upper layer volume transports, allows us to develop, for the first time over the area, a realistic picture of the spatial and temporal variability over a nearly 5-year period, 1992 to 1997.

The SLA variability clearly emphasizes three ranges of variability. The intraseasonal variability is associated with propagating features along the northern part of the area. The mean propagation velocity is consistent with a first off-equatorial baroclinic Rossby wave characteristic. The seasonal variability, which accounts for the largest part in terms of energy, mostly describes the NECC seasonal cycle, in response

to wind forcing. However, more interesting is the appearance of a clear year-to-year variability, with a linear negative trend at the beginning of the period (1992 to the end of 1994), then the occurrence of two events, lasting for several months and beginning first in late boreal summer 1995, then in late spring 1996. This large timescale variability is mostly confined to the northernmost part of the area.

The surface currents also revealed an intraseasonal tendency, with a clear peak of energy at 62 days in the zonal and meridional velocity spectra averaged along 5°N. Larger-scale variability (seasonal to interannual) is mostly zonal, the peak at 360 days being twice as energetic for the zonal component as for the meridional velocity.

The transport across 38°W and between 3°N and 9°N (NECC region) shows a regular seasonal oscillation, in agreement with previous studies, with maximal eastward values in boreal summer-fall season and minimal and westward values in boreal spring. Most of this seasonal variability is due to the 3°N-6°N region, where the southern edge of the NECC is encountered, opposite of the SEC, and seasonally migrates. Year-to-year variations are also evident. The eastward transport loses about 35% of its strength in the second half of 1995 compared with 1994. This event is followed by a stronger than usual westward transport in early 1996. Then, in boreal fall 1996 the situation returns to normal, but in early 1997 the transport seems abnormally eastward. Contrary to the seasonal cycle, this interannual variability is due to the 6°N-9°N band. Meridional transport as computed across 7°30'N and between 50°W and 35°W is northward during the whole period 1992-1995. A seasonal cycle can be detected with maximum transport during boreal winter and minimum in spring; but an interesting result is the increase of the northward transport in April 1993 until boreal fall 1995, where the maximum value for the period is reached.

All these results strongly suggest that the ETAMBOT cruises were carried out during "abnormal" situations. Therefore their very interesting results are more representative of a specific temporal situation in 1995-1996 than of a seasonal contrast between boreal fall and spring.

Complementary work is necessary to investigate the different dynamics evidenced here. Propagating wave-like structures along 7°N could be studied in comparison to *McClean and Klinck*'s [1995] numerical study. Resulting effects of the large-scale interannual variability on net heat and mass fluxes, by comparison to surface events evidenced here, could be investigated, using a complete set of in situ, satellite, and modeling approaches.

Acknowledgments. The authors wish to thank all the colleagues who, with their remarks and suggestions, contributed to this paper: N. Sennechal, E. Kestenare, M.H. Radenac, S. Wacongne, and G. Reverdin. Special thanks to the other "ETAMBOT" colleagues, who are not coauthors of this paper, but without whom the ETAMBOT cruises could not have been carried out : C. Oudot, C. Andrié, J.M. Boré, F. Marin, J.F. Ternon, F. Baurand, and P. Fournier..., and to W.E. Johns and R.E. Zantopp for providing the STACS mooring data. The authors are also grateful to Y. Ménard, M. Lefèvre, and J.F. Minster for their efforts to make the TOPEX/POSEIDON project a success among French oceanographers and for their helpful comments on the TOPEX/POSEIDON data and to J. Merle (IRD) for his leadership role in early tropical Atlantic studies. Part of this work was funded by the French Programme National d'Etudes de la Dynamique du Climat (PNEDC). The authors were supported by the Institut de Recherche pour le Développement (IRD) (formerly ORSTOM).

References

Andrié, C., J.F. Ternon, B. Bourlès, Y. Gouriou, and C. Oudot, Tracer distribution and deep circulation in the western tropical Atlantic during CITHER 1 and ETAMBOT cruises, 1993-1996, *J. Geophys. Res.*, this issue.

Arnault, S., and R.E. Cheney, Tropical Atlantic sea level variability from Geosat (1985-1989), *J. Geophys. Res., 99*, 18,207-18,223, 1994.

Arnault, S., and C. LeProvost, Regional identification in the tropical Atlantic ocean of residual tide errors from an empirical orthogonal function analysis of the TOPEX/Poséïdon altimetric data, *J. Geophys. Res., 102*, 21,011-21,036, 1997.

Arnault, S., Y. Ménard, and J. Merle, Observing the Tropical Atlantic Ocean in 86-87 from altimetry, *J. Geophys. Res., 95*, 17,921-17,945, 1990.

Bauer E., S. Hasselman, K. Hasselman, and H.C. Graber, Validation and assimilation of Seasat altimeter wave heights using tha WAM wave model, *J. Geophys. Res., 97*, 12,671-12,682, 1992.

Blanke, B., and P. Delecluse, Variability of the tropical Atlantic ocean simulated by a general circulation model with two different mixed-layer physics, *J. Phys. Oceanogr., 23*, 1363-1388, 1993.

Bourlès, B., R.L. Molinari, E. Johns, W.D. Wilson, and K.D. Leaman, Upper layer currents in the western tropical North Atlantic (1989-1991), *J. Geophys. Res, 104*, 1361-1376, 1999.

Bourlès, B., Y. Gouriou, and R. Chuchla, On the circulation in the upper layer of the western equatorial Atlantic, *J. Geophys. Res.*, this issue.

Bretherton, F., R. Davis, and C. Fandry, A technique for objective analysis and design of oceanographic experiments applied to MODE-73, *Deep Sea Res., 23*, 559-582, 1976.

Bryan, F.O., I. Wainer, and W.R. Holland, Sensitivity of the tropical Atlantic circulation to specification of wind stress climatology, *J. Geophys. Res., 100*, 24,729-24,744, 1995.

Candela, J., R.C. Beardsley, and R. Limeburner, Separation of tidal and subtidal currents in ship-mounted acoustic Doppler current profiler (ADCP) observations, *J. Geophys. Res., 97*, 769-788, 1992.

Carton, J.A, Estimates of sea level in the tropical Atlantic ocean using Geosat altimetry, *J. Geophys. Res., 94*, 8029-8039., 1989.

Carton, J.A, Tropical Atlantic eddies collide with the the coast of South America (abstract), *Eos Trans. AGU, 72*(51), Ocean Sci. Meet. Suppl., 22, 1991.

Carton, J.A., and E.J. Katz, Estimates of the zonal slope and seasonal transport of the Atlantic North Equatorial Countercurrent, *J. Geophys. Res., 95*, 3091-3100, 1990.

Csanady, G.T., A zero potential vorticity model of the North Brazilian coastal current, *J. Mar. Res., 43*, 553-579, 1985.

Davis, R.E., Predictability of sea surface temperature and sea level pressure anomalies over the North Pacific Ocean, *J. Phys. Oceanogr., 6*, 249-266, 1976.

De Mey, P., and A.R. Robinson, Simulation and assimilation of satellite altimeter data at the oceanic mesoscale, *J. Phys. Oceanogr., 17*, 2280-2293, 1987.

Didden, N., and F. Schott, Seasonal variations in the western tropical Atlantic: surface circulation from Geosat altimetry and WOCE model results, *J. Geophys. Res., 97*, 3529-3541, 1992.

Didden, N., and F. Schott, Eddies in the North Brazil Current retroflection region observed by Geosat altimetry, *J. Geophys. Res., 98*, 20,121-20,131, 1993.

Duchêne, C., and C. Frankignoul, Seasonal variations of surface dynamic topography in the tropical Atlantic: Observational uncertainties and model testing, *J. Mar. Res., 49*, 223-247, 1991.

Du Penhoat, Y., and A.M. Tréguier, The seasonal linear response of the tropical Atlantic Ocean, *J. Phys. Oceanogr., 15*, 316-329, 1985.

Friedrich, M.A.M., and M.M. Hall, Deep circulation in the tropical north Atlantic, *J. Mar. Res., 51*, 697-736, 1993.

Garzoli, S.L., The Atlantic North Equatorial Countercurrent: Models and observations, *J. Geophys. Res., 97*, 17,931-17,946, 1992.

Garzoli, S.L., and A.L. Gordon, Origins and variability of the Benguela current, *J. Geophys. Res., 101*, 897-906, 1996.

Garzoli, S.L. and P.L. Richardson, Low frequency meandering of the North Equatorial Countercurrent, *J. Geophys. Res., 94*, 2079-2090, 1989.

Garzoli, S.L., G.J. Goni, A.J. Mariano, and D.B. Olson, Monitoring the upper southeastern Atlantic transports using altimeter data, *J. Mar. Res., 55*, 3, 453-481, 1997.

Gill, A.E., *Atmosphere-Ocean Dynamics*, *Int. Geophys. Ser.*, vol. 30, 662 pp., Academic, San Diego, Calif., 1982.

Goni, G., S. Kamholz, S. Garzoli, and D. Olson, Dynamics of the Brazilvinas Confluence based on inverted echo sounders and altimetry, *J. Geophys. Res., 101*, 16,273-16,289, 1996.

Gordon, A.L., Interocean exchange of thermocline water, *J. Geophys. Res., 91*, 5037-5046, 1986.

Gouriou, Y., B. Bourlès, H. Mercier, and R. Chuchla, Deep jets in the equatorial Atlantic Ocean, *J. Geophys. Res.*, this issue.

Johns, W.E., T.N. Lee, F.A. Schott, R.J. Zantoff, and R.H. Evans, The North Brazil Current Retroflection: Seasonal structure and eddy variability, *J. Geophys. Res., 95*, 22,103-22,120, 1990.

Johns, W.E., T.N. Lee, R.C. Beardsley, J. Candela, R. Limeburner, and B. Castro, Annual cycle and variability of the North Brazil Current, *J. Phys. Oceanogr., 28*, 103-128, 1998.

Katz, E.J., An interannual study of the Atlantic North Equatorial CounterCurrent, *J. Phys. Oceanogr., 23*, 116-123, 1993.

Le Groupe ETAMBOT, Campagne ETAMBOT 1 N.O. LE NOROIT (9 septembre - 11 octobre 1995), vol 1, *Doc. Sci., 22*, 429 pp., Cent. IRD de Cayenne, Cayenne, French Guiana, 1997a.

Le Groupe ETAMBOT, Campagne ETAMBOT 2 N.O. EDWIN LINK (12 avril - 16 mai 1996), vol 1, *Doc. Sci., 24*, 521 pp., Cent. IRD de Cayenne, Cayenne, French Guiana, 1997b.

Levitus, S., R. Burgett, and T.P. Boyer, World ocean atlas 1994, Vol. 3, Salinity, *NESDIS Atlas 3*, 99 pp., Nat. Oceanic and Atmos. Admin., Silver Spring, Md., 1994.

Levitus, S., and T.P. Boyer, World ocean atlas 1994, Vol. 4, Temperature, *NESDIS Atlas 4*, 117 pp., Nat. Oceanic and Atmos. Admin., Silver Spring, Md., 1994.

Lorentz, E.N., Studies of atmospheric predictability, Final report period March 1966-January 1969, *Rep. AFCRL-69-0119*, 142 pp., Dep. of Meteorol., Mass. Inst. of Technol., Cambridge, 1969.

Mallardé, J.P., P. De Mey, C. Perigaud and J.F. Minster, Observation of long equatorial waves in the Pacific Ocean by Seasat altimetry, *J. Phys. Oceanogr., 17*, 2273-2279, 1987.

Mayer, D.A., and R.H. Weisberg, A description of COADS surface meteorological fields and the implied Sverdrup transports for the Atlantic ocean from 30°S to 60°N, *J. Phys. Oceanogr., 23*, 2201-2221, 1993.

McClean, J.L., and J.M. Klinck, Description and vorticity analysis of 50-day oscillations in the western tropical region of the CME model, *J. Phys. Oceanogr., 25*, 2498-2517, 1995.

Ménard, Y., Observing the seasonal variability in the tropical Atlantic from altimetry, *J. Geophys. Res., 93*, 13,947-13,978, 1988.

Merle, J., and S. Arnault, Seasonal variability of the surface dynamic topography in the tropical Atlantic ocean, *J. Mar. Res., 43*, 2, 267-288, 1985.

Oudot, C., J.F. Ternon, C. Andrié, E. Santis Braga, and P. Morin, On the crossing of the equator by intermediate water masses in the western Atlantic Ocean: Identification and pathways of Antartic Intermediate Water and Upper Circumpolar Water, *J. Geophys. Res.*, this issue.

Philander, S.G.H., Unusual conditions in the tropical Atlantic ocean in 1984, *Nature*, 322, 236-238, 1986.

Philander, S.G.H., and R.C. Pacanowski, A model of the seasonal cycle in the tropical Atlantic ocean, *J. Geophys. Res., 91*, 14,192-14,206, 1986.

Richardson, P.L., and T. McKee, Average seasonal variation of the Atlantic Equatorial currents from historical ship drifts, *J. Phys. Oceanogr., 14*, 1226-1238, 1984.

Richardson, P.L., G. Hufford, R. Limeburner, and W.S. Brown, North Brazil Current retroflection eddies, *J. Geophys. Res., 99*, 5081-5093, 1994.

Schott, F.A., and C.W. Boning, The WOCE model in the western Atlantic upper layer circulation, *J. Geophys. Res., 96*, 6993-7004, 1991.

Schott, F. A., L. Stramma, and J. Fischer, Transports and pathways of the upper-layer circulation in the western tropical Atlantic, *J. Phys. Oceanogr., 28*, 1904-1928, 1998.

Von Storch, H., and A. Navarra, *Analysis of Climate Variability: Applications of Statistical Techniques*, 335 pp., Springer-Verlag, New York, 1993.

S. Arnault, Laboratoire d'Océanographie Dynamique et de Climatologie, Unité Mixte de Recherche 7617 CNRS/IRD/Université Pierre et Marie Curie, Tour 14-2, case 100, 4 place Jussieu, 75252 Paris Cedex 05, France. (sa@lodyc.jussieu.fr)

B. Bourlès, Y. Gouriou, and R. Chuchla, Centre Institut de Recherche pour le Développement de Brest, Plouzané, France.

(Received April 20, 1998; revised April 12, 1999;
accepted April 16, 1999.)